University of Barcelona
Master in Quantum Science and Technology

Master's thesis

Experimental Setup For Measuring The Bell Inequalities

Universitat de Barcelona

This project has received funding from the European Union's Digital Europe Programme under grant agreement no. 101084035.

Raúl Lahoz Sanz[†]
Directors: Bruno Julia Diaz and José María Gómez Cama

Course 2022–2023

[†]rlahozsanz@icc.ub.edu

Experimental Setup For Measuring The Bell Inequalities

Raul Lahoz Sanz

Supervised by: Bruno Julia Diaz & José María Gómez Cama

Facultad de Física UB (ICCUB), 08028 Barcelona

10 July 2023

This master thesis centers on the construction, development and characterization of an experimental setup to demonstrate quantum nonlocality using polarization-entangled photons through a Bell Test. The generation of polarization-entangled photon pairs is accomplished through Type-I Spontaneous Parametric Down-Conversion (SPDC), using a pair of Beta Barium Borate (BBO) crystals.

The thesis explores the theoretical foundations of SPDC and describes the assembly and alignment process of the system to obtain entangled photon pairs.

A significant violation of Bell's inequalities is observed with a confidence level around 4-σ. This violation is demonstrated using two different entangled states, providing empirical evidence for the existence of non-local correlations beyond classical theories, supporting the principles of quantum mechanics.

Acknowledgements

This study was supported by MCIN with funding from European Union NextGenerationEU (PRTR-C17.I1) and by Generalitat de Catalunya.
Now, I would like to thank all those individuals who have made my work possible by supporting and advising me at every step of the way.

First and foremost, I extend my appreciation to my colleagues Lidia Lozano, Kristian Feliz and Adrià Brú i Cortés for their contributions to discussions related to quantum entanglement.

I would also like to thank Martí Duocastella and his team for their insights regarding optical concepts and devices. In addition, I want to show my appreciation to Radek Łapkiewicz for his generosity and useful tips on how to improve our experimental setup.

Moreover, I want to express my appreciation to Morgan Mitchell for the various discussions about our setup, his enlightening talks about the concept of quantum entanglement and his valuables advices.

Finally, I am deeply thankful to my supervisors Bruno Julia Diaz and José María Gómez Cama for their exceptional guidance and invaluable assistance throughout these months. Their expertise, dedication and the trust they have placed in me to carry out this project.

Raul Lahoz Sanz: rlahozsanz@icc.ub.edu

Contents

This work is organized as follows: In Sec. 1, we present a brief historical introduction of the key concepts in this work, as well as the current state of this field of knowledge. In Sec. 2, we present our motivations for conducting this experiment. In Sec. 3, we set the objectives of the project. In Sec. 4, we discuss the generation of entangled photons through the SPDC process. In Sec. 5, we study the theory behind the CHSH inequality. In Sec. 6, we describe our experimental setup. In Sec. 7, we outline the steps we have taken to obtain entangled photon pairs at the output of the BBO crystals. In Sec. 8, we characterize the entanglement of our photons and perform the Bell Test. Finally, in Sec. 9, we present the conclusions of our work and some suggestions for improving it.

1 Introduction

The concept of quantum entanglement was used in 1935 by Einstein, Podolsky, and Rosen as an argument to attack quantum mechanics by claiming that it was an incomplete description of reality [EPR35]. According to Albert Einstein's theory of relativity, any communication or influence between two objects separated by any distance cannot be transmitted at a speed higher than the one of light. Therefore, the idea that two entangled particles could instantaneously influence each other seemed to disprove this theory.

In 1964, John S. Bell proposed his famous inequalities providing a way to solve the conundrum about the interpretation of quantum mechanics [Bel64]. The Bell inequalities were developed a priori as a way to test the validity of local realism, a view of the physical world that suggests that particles have pre-existing, defined properties that determine their behavior. It was a significant breakthrough in the field of quantum mechanics, as Bell's work demonstrated that local realism is incompatible with the predictions of quantum mechanics, which means that there is a fundamental difference between the classical and the quantum domain, and it can be experimentally proven.

The first experiment to test Bell's inequalities was performed by physicist John Clauser and his colleagues in 1972 and is commonly known as the Clauser-Horne-Shimony-Holt (CHSH) experiment [CHSH69, FC72]. This experiment demonstrated that the predictions of quantum mechanics were correct and that local realism, a fundamental assumption in classical physics, was incorrect in the quantum world. Since then, numerous additional experiments have confirmed Bell's inequalities and established the fundamentally non-local nature of quantum mechanics.

Nowadays, the topic of quantum entanglement holds great significance, evident by the awarding of the 2022 Nobel Prize in Physics to researchers Alain Aspect [ADR82, AGR82], John Clauser [FC72], and Anton Zeilinger [WJS+98, BPM+97]. Their groundbreaking experiments with entangled photons and pioneering contributions to the field of quantum information science have garnered them this prestigious recognition.

2 Motivation

Currently, the construction of an experimental setup to measure the violation of Bell inequalities in pairs of entangled photons is of utmost importance. With the growing interest and demand for the use of entangled photons in numerous applications such as quantum teleportation [BBC+93], super dense coding [BW92] or quantum key distribution (QKD) [BB14] among others, there is an urgent need to verify if two photons are quantum entangled. This is where the Bell Test comes into play.

Our experimental setup offers a robust and simple solution for performing these fundamental measurements. It has been designed with simplicity and precision in mind, making

it accessible for students in lower-level physics courses to assemble and use in their undergraduate laboratories.

The possibility of introducing this experimental setup as a laboratory practice not only stimulates hands-on learning but also provides students with the opportunity to directly experiment with complex theoretical concepts. By allowing them to perform measurements and obtain tangible results, a greater understanding of quantum phenomena is promoted, strengthening their foundation in quantum physics.

3 Objectives

We seek to assemble an experimental setup for measuring the Bell inequalities in pairs of entangled photons generated using BBO crystals. For this purpose, we take as reference the experiment conducted by Dietrich Dehlinger and Morgan W. Mitchell [DM02a, DM02b]. Additionally, we try to make it more robust and accessible so that it can be used as a laboratory practice for undergraduate students in physics courses.
Our objectives are:

- Find the points in space where the detectors detect the highest number of coincident counts. Once the detectors are fixed at these positions, determine the optimal position of the BBO crystals for generating photon pairs in maximally entangled states.
- Discern whether the photon pairs produced by our BBO crystal are entangled or not and characterize the degree of entanglement by performing the Bell Test.
- Understand the generation of entangled photons within our BBO crystals, as well as the influence of the rotation angle of our BBO crystal on the wave function of the photon pairs.

4 Generation of entangled photons

In quantum physics, an entangled state is a state whose associated wave function cannot be factorized in terms of the states of the individual subsystems independently. Thus, in an entangled state, the properties of the individual subsystems cannot be completely separated and are inherently linked to each other and according to the Copenhagen interpretation, any measurement performed on one of the subsystems will instantaneously affect the other, regardless of the distance that separates them.

We can think of an entangled state in polarization between two photons as the state $\frac{1}{\sqrt{2}}(|VV\rangle + |HH\rangle)$ where neither of the two particles has a predefined polarization, but the act of measuring the polarization of one of them allows us to instantaneously and precisely determine the polarization of the other, even if they are separated by great distances.

The production of polarized-entangled photons is carried out using a pair of BBO crystals. To do this, we take advantage of the phenomenon known as spontaneous parametric downconversion (SPDC), through which an incident photon (pump photon) is converted into two photons (idler and signal photons) inside a BBO crystal [Cou18].

During the SPDC process, a high-intensity pump with angular frequency ω_p is incident on a second-order nonlinear optical crystal, which spontaneously splits into pairs of lower energy (longer wavelength) photons (signal, ω_s, and idler, ω_i).

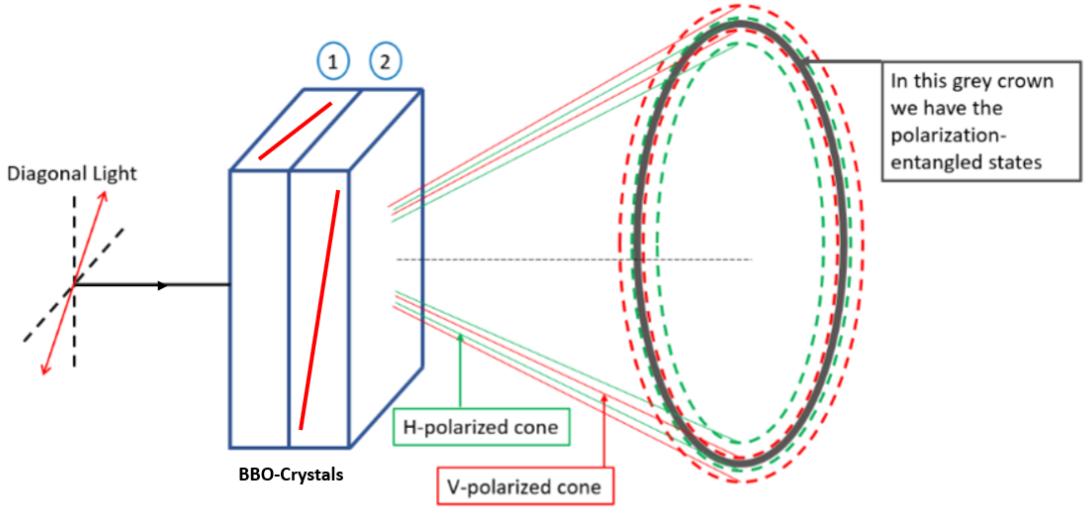

Figure 1: Entangled photon production scheme using Type-I SPDC with two BBO crystals. The red lines in each crystal indicate the direction of the optical axis inside them.

Energy and momentum conservation throughout the process imply,

$$\omega_p = \omega_s + \omega_i, \tag{1}$$

$$\vec{k_p} = \vec{k_s} + \vec{k_i}, \tag{2}$$

that is, the energy (momentum) of the incident photon must be equal to the sum of the energies (momenta) of the two photons that have been produced in the process.
From $\vec{k_p} = \vec{k_s} + \vec{k_i}$ we can draw two conclusions. The first one is that the three vectors $\vec{k_p}$, $\vec{k_s}$ and $\vec{k_i}$ lie in a plane, and the second one is that the photons generated by SPDC with degenerate energy ($\omega_s = \omega_i$) exit the BBO crystal both at the same angle with respect to the propagation direction of the incident pump beam, as

$$k = \frac{2\pi}{\lambda} = \frac{\omega}{c}. \tag{3}$$

Then, for the generation of entangled photons, we use the same method as [DM02a, DM02b], that is two BBO crystals in contact face to face and one of them rotated 90°[1] with respect to the other, see Fig. 1.

When a photon goes through a crystal, with a low probability (one in a million) SPDC occurs, and the incident photon with extraordinary polarization gives rise to two photons, both with ordinary polarization [KWW+99].

Thus, in Fig. 1, incident photons with horizontal (vertical) polarization give rise to pairs of photons with vertical (horizontal) polarization in the first (second) crystal. As there is no preferred direction of propagation for the pairs of photons produced by SPDC, we have that at the output of the pair of BBO crystals, we have two cones of light, one with vertically polarized photons and the other with horizontally polarized photons. If we cut these cones of light with a plane perpendicular to the axis of symmetry of the cones, we find the pairs of photons generated in the crystals diametrically opposed on the ring of light that is formed in that plane.

[1]The rotation is performed along the axis that has the same direction as the incident pump photons

By shinning the BBO crystals with diagonally polarized pump photons, that is, photons that are in an equal superposition of states $|V\rangle$ and $|H\rangle$ ($|\Psi\rangle = {}^1/\sqrt{2}\,(|V\rangle + |H\rangle)$). If a photon downconverts in the scheme of Fig. 1 and those photons generated propagate in the region where both light cones overlap, then we have two photons that are either both vertically polarized or both horizontally polarized but neither has a known polarization until it is measured. If we measure one of them we know perfectly the state of the other. That's precisely what it means to be entangled.

So we find the entangled photons in the region of space where the vertically polarized and the horizontally polarized cones of light overlap. This is because in this region, we do not know beforehand in which of the two crystals the pair of photons has been generated. That is, the photons produced in the first crystal and the photons produced in the second crystal are indistinguishable at this point in space. Therefore, our state is a superposition of both cases.

4.1 Analytical expression of the SPDC wave function

Once we have introduced how SPDC occurs inside a crystal, we will obtain the analytical expression of the wave function in terms of the angle θ of rotation of the BBO crystals.

For convenience, we use the rotated polarization basis $\{|V_\alpha\rangle, |H_\alpha\rangle\}$. By convention, we take the counterclockwise direction as the positive direction for angles when we observe the light propagating toward us. Therefore, in Fig. 2 (a), we are seeing the light propagating towards us. The relationship between the basis $\{|V_\alpha\rangle, |H_\alpha\rangle\}$ and the basis $\{|V\rangle, |H\rangle\}$ is:

$$\begin{cases} |V_\alpha\rangle = \cos(\alpha)\,|V\rangle - \sin(\alpha)\,|H\rangle \\ |H_\alpha\rangle = \sin(\alpha)\,|V\rangle + \cos(\alpha)\,|H\rangle \end{cases} \tag{4}$$

Now, let's assume that in our scenario, we shine the BBO crystals with a horizontally polarized 405 nm beam. Furthermore, we also assume that for $\theta = 0°$, the planes of the optical axis are arranged in the directions given by the vectors $|H_{45°}\rangle$ (Plane $\mathrm{SPDC}_{\mathrm{BBO}_1}$) and $|V_{45°}\rangle$ (Plane $\mathrm{SPDC}_{\mathrm{BBO}_2}$), as shown in Fig. 2 (b).

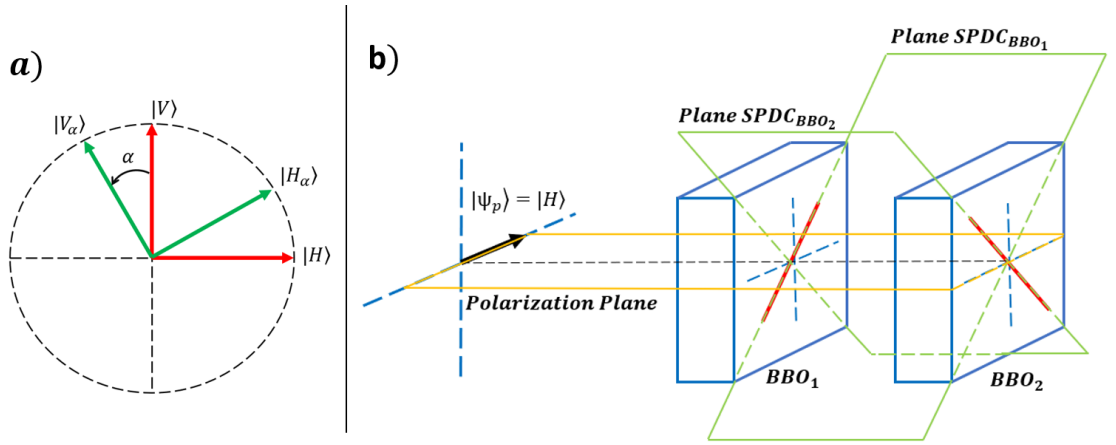

Figure 2: (a) Representation of $\{|V_\alpha\rangle, |H_\alpha\rangle\}$ and $\{|V\rangle, |H\rangle\}$ basis. (b) Visual representation of the planes. Planes $\mathrm{SPDC}_{\mathrm{BBO}_1}$ and $\mathrm{SPDC}_{\mathrm{BBO}_2}$ are formed by the optical axis (red lines inside each BBO crystal) of the first and second BBO-crystal respectively and the direction of the 405 nm beam (dashed black line). Polarization Plane is formed by the polarization of the 405 nm beam and its propagation direction. In this representation, the planes $\mathrm{SPDC}_{\mathrm{BBO}_1}$ and $\mathrm{SPDC}_{\mathrm{BBO}_2}$ are perpendicular to each other, and each of them forms a $45°$ angle with the polarization plane.

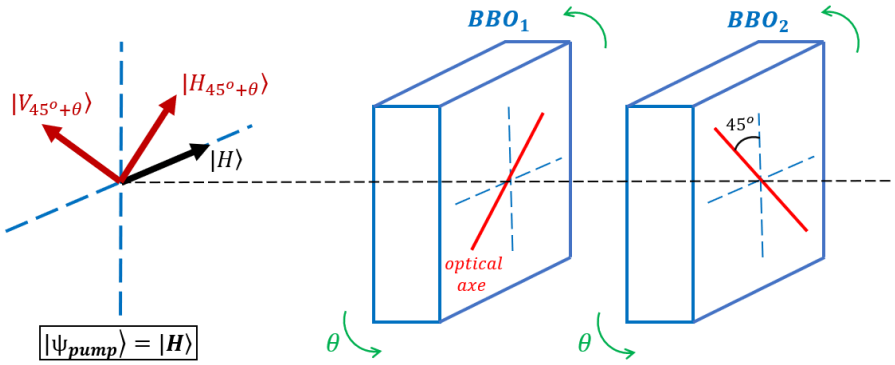

Figure 3: SPDC production scheme as a function of the angle θ of our BBO crystals. The BBO crystals are shown separated in the image for better visibility of how the optical axis are arranged inside them, but in the laboratory, they are in direct contact face to face.

Since we know that for SPDC to occur, the polarization of our photon must lie in the plane formed by the crystal's optical axis and the photon's propagation direction, for convenience, we rewrite the wave function of the pump photons in the basis $\{|V_{45°+\theta}\rangle, |H_{45°+\theta}\rangle\}$. In other words,

$$|\Psi_{\text{Pump}}\rangle = \cos(45° + \theta)\,|H_{45°+\theta}\rangle - \sin(45° + \theta)\,|V_{45°+\theta}\rangle\,. \tag{5}$$

Thus, the probability of SPDC occurring in the first (second) crystal is proportional to the squared modulus of the projection of the state $|\Psi_{\text{Pump}}\rangle$ onto the vector $|H_{45°+\theta}\rangle$ ($|V_{45°+\theta}\rangle$), which defines the direction of the plane $\text{SPDC}_{\text{BBO}_1}$ ($\text{SPDC}_{\text{BBO}_2}$), see Fig. 3. Then,

$$P^{\text{SPDC}}_{\text{BBO}_1} \propto |\langle\Psi_{\text{Pump}}|H_{45°+\theta}\rangle|^2 = \cos^2(45° + \theta),$$
$$P^{\text{SPDC}}_{\text{BBO}_2} \propto |\langle\Psi_{\text{Pump}}|V_{45°+\theta}\rangle|^2 = \sin^2(45° + \theta).$$

We can observe that in the first crystal, when SPDC occurs, we have a transition from a photon $|H_{45°+\theta}\rangle$ to two photons $|V_{45°+\theta}\rangle\,|V_{45°+\theta}\rangle$. On the other hand, in the second crystal, when SPDC takes place, we have a transition from a photon $|V_{45°+\theta}\rangle$ to two photons $|H_{45°+\theta}\rangle\,|H_{45°+\theta}\rangle$. In other words, when SPDC occurs inside a BBO crystal, a pump photon with polarization contained in the plane formed by its propagation direction and the crystal's optical axis transforms into two photons, being the polarization of these photons orthogonal to that of the pump photon that suffered SPDC.

Now we consider the relative phase that appears between the components $|V_{45°+\theta}\rangle\,|V_{45°+\theta}\rangle$ and $|H_{45°+\theta}\rangle\,|H_{45°+\theta}\rangle$, as the photon pairs pass through different optical paths inside the BBO crystals [AJK05]. In the first crystal, photons with the polarization direction $|V_{45°+\theta}\rangle$ propagate according to the crystal's ordinary refractive index, while photons with the polarization direction $|H_{45°+\theta}\rangle$ propagate according to the effective refractive index $n^{\text{eff}}(\alpha)$. For the second crystal, since it is rotated by 90° relative to the first crystal, the situation is completely opposite. Photons with the polarization direction $|H_{45°+\theta}\rangle$ propagate according to the crystal's ordinary refractive index, while photons with the polarization direction $|V_{45°+\theta}\rangle$ propagate according to the effective refractive index $n^{\text{eff}}(\alpha)$.

$$n^{\text{eff}}(\alpha) = \sqrt{\frac{1}{\frac{\cos^2\alpha}{n_e^2} + \frac{\sin^2\alpha}{n_o^2}}} \tag{6}$$

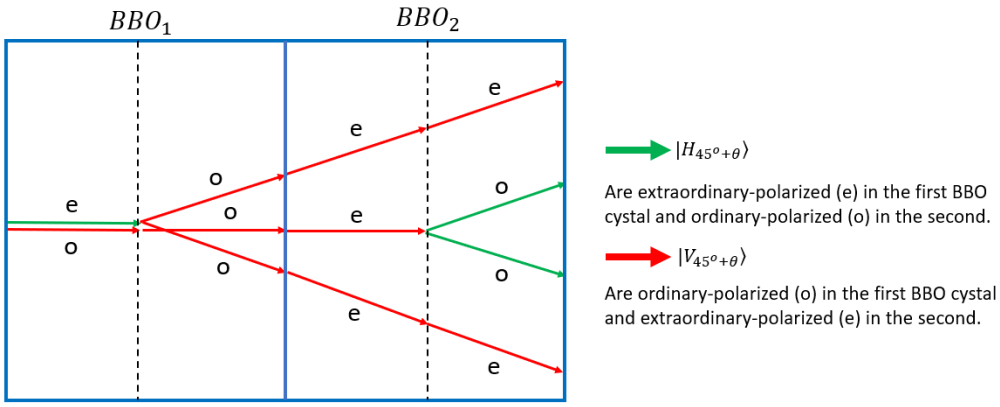

Figure 4: Optical path scheme followed by photons that suffer SPDC when passing through the BBO crystals. The BBO crystals in this illustration are cut by the detection plane, see Fig. 8. The propagation directions of both the pump photons and the signal and idler photons are also contained in this detection plane.

Where α is the angle between the optical axis of the crystal and the propagation direction of the photons with extraordinary polarization. We know that downconverted photons are ordinarily polarized in the crystals where they are generated and extraordinarily polarized in the other crystal. Thus, assuming that the "signal" and "idler" photons are generated in the center of their respective crystals and travel in completely symmetrical directions with respect to the pump beam, we construct the schematic representation of the optical path of photons with propagation directions contained in the detection plane (see Fig. 8) inside the BBO crystals, see Fig. 19.

Notice that when the pair of photons generated in the first crystal pass through the second crystal, both the "signal" and "idler" photons have the polarization contained in the plane of the optical axis and then they propagate with an effective refractive index of $n^{\text{eff}}(\alpha_s(\theta))$ and $n^{\text{eff}}(\alpha_i(\theta))$ respectively. Where we denote $\alpha_s(\theta)$ $(\alpha_i(\theta))$ as the angle formed by the propagation direction of the signal (idler) photons with the optical axis in the second crystal.

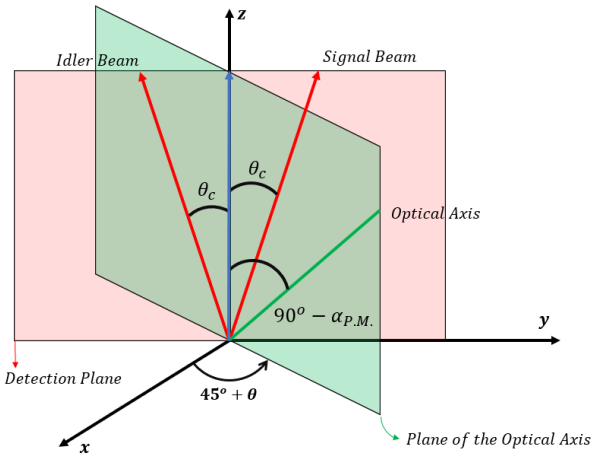

Figure 5: Diagram illustrating the arrangement of planes and the propagation directions of the photons produced by SPDC in the first crystal inside the second BBO crystal. $\alpha_{P.M.}$ is the phase-matching angle of our BBO crystals

Fig. 5 shows the direction of the optical axis as a function of θ and the propagation directions of the downconverted photons inside a BBO crystal. We also observe that the angles $\alpha_s(\theta)$ and $\alpha_i(\theta)$ vary depending on the angle θ of the BBO crystals.

Thus we have a dependence of the optical path followed by the photons with the rotation angle θ as the effective refractive index of the signal and idler photons varies with $\alpha_s(\theta)$ and $\alpha_i(\theta)$. We model our relative phase as a function of the angle θ as the sum of a constant term (ϕ) and a term dependent on the rotation angle of the crystals ($\psi(\theta)$). Therefore, the relative phase between components after going through both BBO crystals is

$$\phi(\theta) = \phi + \psi(\theta). \tag{7}$$

We can finally construct the wave function in terms of the rotation angle θ of the crystals when SPDC occurs in them, simply by substituting in Eq. (5) the terms $|V_{45°+\theta}\rangle \longrightarrow |H_{45°+\theta}\rangle\,|H_{45°+\theta}\rangle$ and $|H_{45°+\theta}\rangle \longrightarrow |V_{45°+\theta}\rangle\,|V_{45°+\theta}\rangle$, and adding the relative phase $\phi(\theta)$ between the two components. See Annex V for the complete calculation of the relative phase between components, even for the case in which the BBO crystals are slightly tilted.

$$|\Psi(\theta)\rangle = \cos(45° + \theta)\,|V_{45°+\theta}\rangle\,|V_{45°+\theta}\rangle - e^{-i\phi(\theta)}\sin(45° + \theta)\,|H_{45°+\theta}\rangle\,|H_{45°+\theta}\rangle\,. \tag{8}$$

5 Bell Test: CHSH inequality

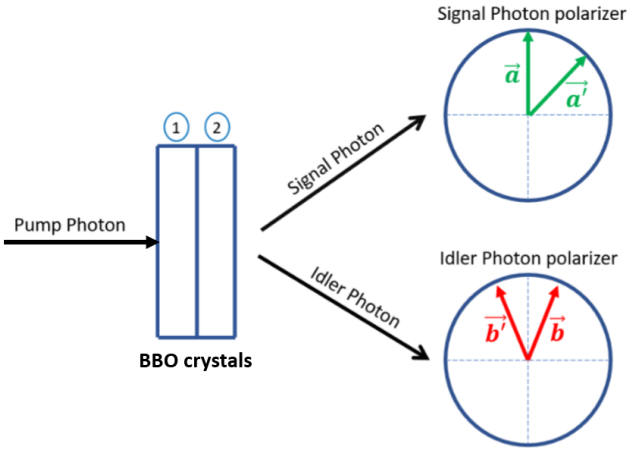

Figure 6: Scenario for the CHSH Bell Test.

The Bell Test is an experiment in which measurements are performed on two particles, and the statistics of the correlations of the outcomes are calculated to determine whether they are compatible with a hidden variables description or a quantum mechanical description. A schematic representation of the CHSH Bell scenario is shown in Fig. 6.

To build the scenario for the CHSH Bell Test described in Fig. 6 we need two polarizers, one in front of the signal photon detector and the other in front of the idler photon detector. For the polarizer in front of the signal photon detector, we assign two different positions $\vec{a}$ ($|V_{0^\circ}\rangle$) and $\vec{a'}$ ($|V_{-45^\circ}\rangle$) while for the polarizer in front of the idler photon detector, we assign another two different positions $\vec{b}$ ($|V_{-22.5^\circ}\rangle$) and $\vec{b'}$ ($|V_{22.5^\circ}\rangle$). Where we have used the $\{|V_\alpha\rangle, |H_\alpha\rangle\}$ basis, see Eq. (4).

When a polarizer is held at a specific angle γ, we assign the value $+1$ to the detected photon that passes through the polarizer (referred to as V_γ), and we assign the value -1 to the detected photon that passes through a polarizer rotated 90° from its original position (referred to as H_γ).

When the signal and idler polarizers are fixed in specific directions $\vec{a}$ and $\vec{b}$ respectively, we encounter four possible combinations: $V_{\vec{a}}V_{\vec{b}}$, $V_{\vec{a}}H_{\vec{b}}$, $H_{\vec{a}}V_{\vec{b}}$, and $H_{\vec{a}}H_{\vec{b}}$. The first and fourth combinations result in an outcome of $+1$, while the second and third combinations yield a result of -1. For a certain arrangement of the two polarizers, we define $E(\vec{a},\vec{b})$ as,

$$E(\vec{a},\vec{b}) = P_{VV}(\vec{a},\vec{b}) - P_{HV}(\vec{a},\vec{b}) - P_{VH}(\vec{a},\vec{b}) + P_{HH}(\vec{a},\vec{b}). \tag{9}$$

To obtain $E(\vec{a},\vec{b})$ we have to perform 4 different measurements. We know that the pairs of photons produced in the BBO crystal are generated at the same instant of time, and therefore, if we place both detectors at the same distance from the BBO crystal, they detect counts at the same instant of time (coincidence counts). We use coincidence detection as a way to discern the downconverted photons from the background of additional photons that reach the detectors.

The way we can measure using coincidence detection the number of pairs of photons that in an entangled state, the signal photon passes through the signal polarizer and the idler photon gets stopped in the idler polarizer for certain directions of the polarizers $\vec{a}$ and $\vec{b}$ ($N_{VH}(\vec{a},\vec{b})$) is to rotate the idler polarizer by 90° from respect to the $\vec{a}$ direction. A similar procedure but rotating the signal polarizer by 90° with respect to the $\vec{b}$ direction

for the case where we want to measure $N_{HV}(\vec{a},\vec{b})$. To measure the number of pairs of photons such that both of them get blocked by their respective polarizers ($N_{HH}(\vec{a},\vec{b})$), we have to rotate both polarizers by 90° with respect to the $\vec{a}$ and $\vec{b}$ directions, respectively.

Note that by using this trick of rotating one (or both) polarizers 90°, we obtain the same statistics as if we were able to detect which photons are stopped by the polarizer(s). Therefore, for a certain arrangement of the two polarizers and repeating the experiment over the same period of time for the four cases we obtain that,

- For the polarizers in the $\vec{a}$ and $\vec{b}$ directions, we obtain $N_{VV}(\vec{a},\vec{b})$.
- For the polarizers in the $\vec{a}+90°$ and $\vec{b}$ directions, we obtain $N_{HV}(\vec{a},\vec{b})$.
- For the polarizers in the $\vec{a}$ and $\vec{b}+90°$ directions, we obtain $N_{VH}(\vec{a},\vec{b})$.
- For the polarizers in the $\vec{a}+90°$ and $\vec{b}+90°$ directions, we obtain $N_{HH}(\vec{a},\vec{b})$.

Since N_{VV}, N_{VH}, N_{HV}, and N_{HH} refer to the number of coincidence counts detected for a specific time interval with the polarizers set at specific positions, we use the following equalities to calculate the associated probabilities,

$$P_{VV}(\vec{a},\vec{b}) = \frac{N_{VV}(\vec{a},\vec{b})}{N_{\vec{a},\vec{b}}}, \qquad P_{VH}(\vec{a},\vec{b}) = \frac{N_{VH}(\vec{a},\vec{b})}{N_{\vec{a},\vec{b}}},$$
$$P_{HV}(\vec{a},\vec{b}) = \frac{N_{HV}(\vec{a},\vec{b})}{N_{\vec{a},\vec{b}}}, \qquad P_{HH}(\vec{a},\vec{b}) = \frac{N_{HH}(\vec{a},\vec{b})}{N_{\vec{a},\vec{b}}},$$

where $N_{\vec{a},\vec{b}} = N_{VV}(\vec{a},\vec{b}) + N_{VH}(\vec{a},\vec{b}) + N_{HV}(\vec{a},\vec{b}) + N_{HH}(\vec{a},\vec{b})$. Thus, by adding these four probabilities we obtain the value of $E(\vec{a},\vec{b})$ as we can see in the Eq. (9). Finally, we define the expectation value of S as:

$$\langle S\rangle = E(\vec{a},\vec{b}) + E(\vec{a'},\vec{b}) + E(\vec{a},\vec{b'}) - E(\vec{a'},\vec{b'}). \tag{10}$$

Its importance arises from the fact that $|\langle S\rangle| \leq 2$ for any HVT model and arbitrary $\vec{a}$, $\vec{a'}$, $\vec{b}$, $\vec{b'}$ (see Annex I). Quantum mechanics statistics can violate this inequality for certain settings (see Annex II).

Obtaining a value of $|\langle S\rangle|$ greater than 2 in the Bell Test supports the validity of quantum mechanics and discredits classical theories that attempt to explain quantum phenomena through local hidden variables. This supports the idea that nature is fundamentally probabilistic and non-local at the quantum level.

Obtaining a value of $|\langle S\rangle|$ less than 2 does not necessarily mean that the system is not entangled. A value of $|\langle S\rangle|$ less than 2 still allows for the possibility of quantum entanglement as it is compatible with both entangled systems that follow the laws of quantum mechanics and systems that follow the laws of hidden variable theories.

6 Description of our setup

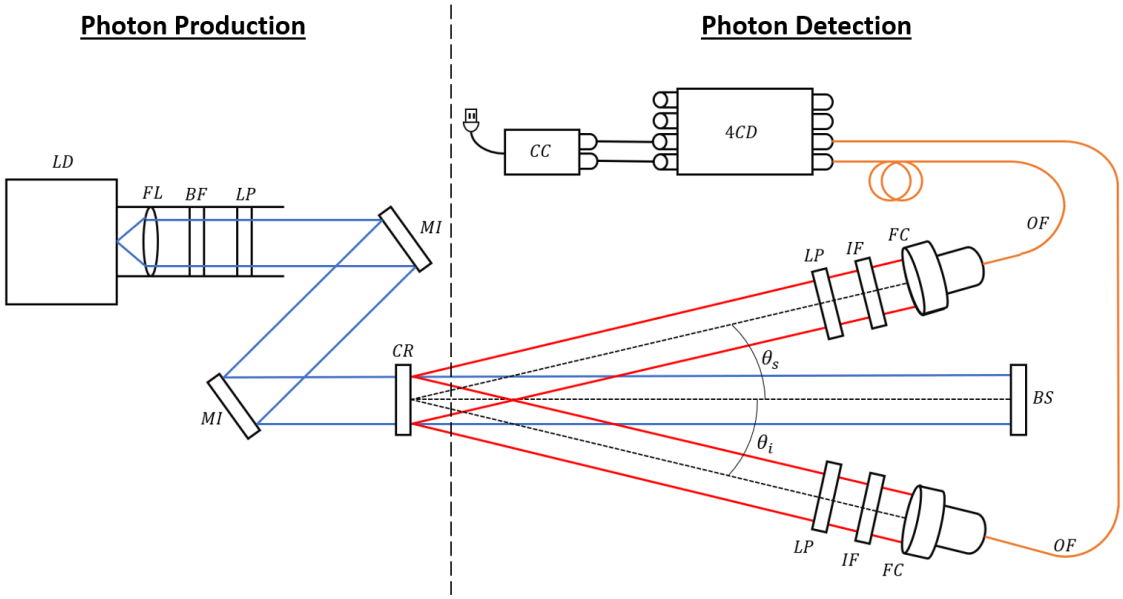

Figure 7: Schematic representation of the setup with all the elements. LD: laser diode. FL: focusing lens. BF: blue filter. LP: linear polarizer. MI: mirror. CR: BBO crystals. IF: infrared filter. FC: fiber coupler lens. BS: beam stop. OF: optical fiber. 4CD: 4-channel detector. CC: coincidence circuit.

Our setup builds on the one used by Alejandro Jaramillo during the development of his Master's Thesis last year [Jar23]. Two of the main changes that have been introduced regarding the previous setup are:

- The use of two mirrors placed in 3D precision mounts to accurately direct the 405 nm beam through the center of the assembly and parallel to the optical table.
- The use of fiber-coupled lenses for photon collection. This also represents a significant improvement in terms of aligning the system as described in the following subsection.

Similarly, our current setup can also be divided into two parts: the photon production part and the photon detection part [Jar23], see Fig. 7.

6.1 Photon production part

The photon production part consists of a 405 nm laser diode with a power of 40 mW, mounted in a temperature-controlled housing. The frontal panel of the casing is equipped with threaded holes to facilitate the installation of a 30 mm cage system. This setup enables the placement of a focusing aspheric lens (f = 4.52 mm), a band-pass filter with a wavelength range of 405 ± 10 nm, and a polarizer inside a rotational mount. Subsequently, the laser light traverses through free space and is reflected by two ∅1" mirrors, each one mounted in a 3D precision mount. With these mirrors, the light travels parallel to the optical table. After this, the light gets into the pair of $6 \times 6 \times 0.1$ mm crystals cut at a phase-matching angle of $\theta = 29.2°$ where photon pairs of approximately 810 nm are generated. These photons exit the crystal at an angle of approximately $\theta_s = \theta_i = 3°$ with respect to the direction of the 405 nm light beam.

6.2 Photon detection part

The photon detection part consists of a pair of identical metallic arms, both arms are able to rotate independently around the BBO crystals. In each arm, we have a linear polarizer, an 800 ± 40 nm band-pass filter, and a fiber coupler lens that collimates light into a multimode optical fiber cable. The photons that have been introduced into the multimode optical fiber travel through it until they reach the 4-channel detector (SPCM-AQ4C), where each of these photons produces an electrical pulse with 50% efficiency. Finally, in order to consider a coincidence detection valid, it is crucial to verify that both photons have arrived at approximately the same time at their respective detectors. For this purpose, these electrical pulses pass through a coincidence circuit. The circuit's output is obtained using a Python program designed by a former student, Martí Pedemonte. The circuit is configured with a coincidence window of 25 nanoseconds, which means that when a photon is detected in one channel, if within a time interval of 25 ns another photon is detected in the other channel, we consider that both photons have arrived simultaneously.

7 Preparation of the entangled state

In this section, we describe the steps we have followed to align our system in order to find:

- The points where the detectors detect the highest number of coincident counts.
- The angles of the BBO crystals for which photon pairs in maximally entangled states are produced.

7.1 Alignment of the system

A key factor in this experiment is the alignment of the system. First, we need to make sure that the 405 nm light beam travels parallel to the optical table so that we can position the polarizers, filters, and coupler lenses at the same height. If we do so, then by fixing the metallic arms on which these elements are mounted, each forming the same angle $\theta_s = \theta_i$ with respect to the 405 nm light beam, we are measuring at diametrically opposite points on the circular light crown that we can observe in Fig. 1. Therefore, we are able to detect coincidences.

To achieve this, we use a pair of mirrors placed in 3D-precision mounts, which allow us to tip and tilt the mirrors in all directions of space, thus precisely directing the light beam through the center of the system and parallel to the optical table. The mirror on which the laser light first reflects is used to direct the light through the center of the setup, in other words, through the bisector of the metal arms, also trying to ensure that the light spot on the second mirror hits at the same height as the detection plane. We refer to the detection plane as the plane parallel to the optical table where the BBO crystals, the 405 nm laser beam (after the reflection in the second mirror) and all the elements of the metal arms (polarizers, filters and fiber collimating lenses) are contained. Finally, with the second mirror, we try to adjust the height of the reflected beam to ensure it travels completely parallel to the table.

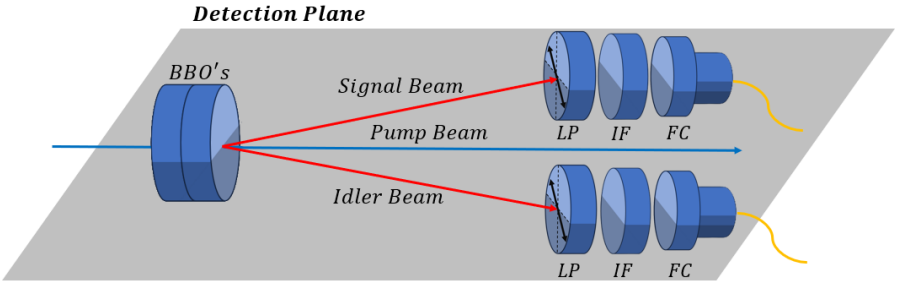

Figure 8: Schematic representation of the detection plane with the pump beam (after the reflection in the second mirror) and all the elements of the metal arms (LP. Linear Polarizers, IF. Infrared Filters and FC. Fiber Collimating lenses) contained on it

Moreover, we need to ensure that the coupler lenses properly couple the light from the BBO crystals into the fiber. Since we are working with optical fibers, this is an aspect that is easy to verify. If we input a light beam through one end of the fiber connected to the 4-channel detector in such a way that the light exits through the end where the lens is placed, making it act as a collimating lens, then, we have a collimated light beam at the output. If we do this simultaneously in both optical fibers and adjust the trajectories of the light beams so that the 405 nm beam and these two beams from the fibers intersect at the same point, we know that if we place the BBO crystals at that point, we are capturing in both fibers all the photons produced in this point that reach the coupler lenses.

7.2 Optimal rail angles between observed photons

First, the most important thing in this experiment is to have the highest possible number of coincident counts, as if we do not have a number of coincident counts at least one order of magnitude larger than the number of coincident counts we would expect to find by mere chance, we cannot ensure that the coincident photons we are detecting are originated in the BBO crystal. To estimate the number of coincident counts we would expect to obtain if detectors A and B detect a number of individual counts N_A and N_B respectively, within a time interval T, we use the equation

$$N_{acc} = \frac{N_A \cdot N_B \cdot \tau}{T}, \tag{11}$$

where τ is the time corresponding to the detection window, in our case 25 ns.

To find the point where we detect the highest number of coincident counts, we place a metal rail (and therefore a detector) at a certain angle with respect to the 405 nm laser beam while varying the angle of the other metal rail. To take this measurement, we remove the polarizers that are placed on the metal rails, thus maximizing the number of coincident counts reaching our detectors, as we are not measuring the polarization of the photon pairs at any moment and therefore collapsing their corresponding wave function.

To carry out this experiment, we perform the detailed study mentioned above for 6 different angles of the fixed rail, see Fig. 9. In this way, we can determine the optimal position of the rails to detect a maximum number of coincident counts.

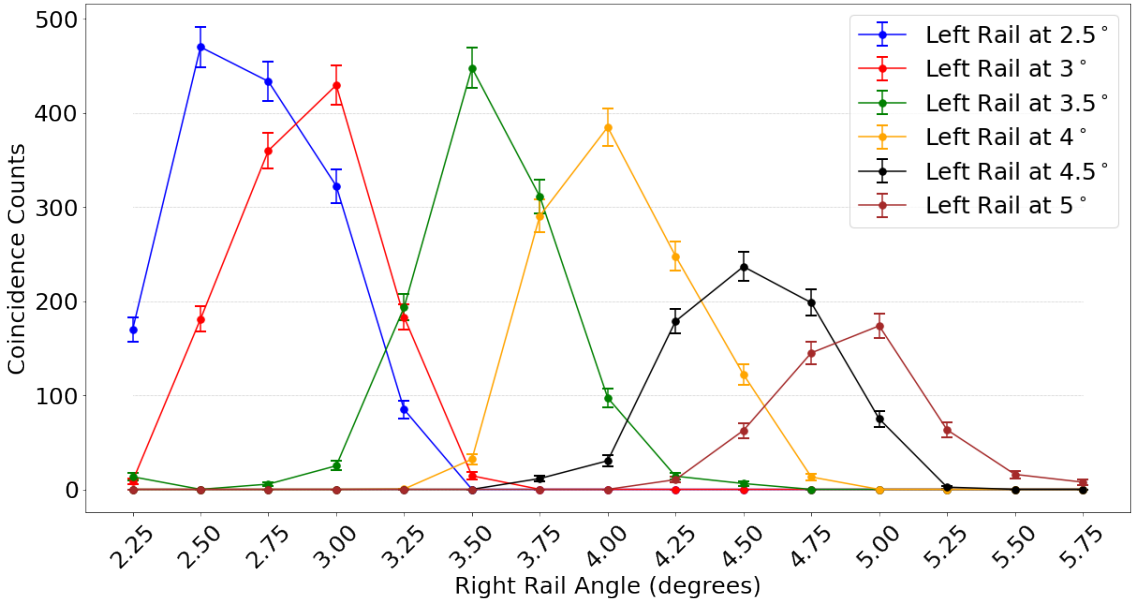

Figure 9: Coincidence counts detected by varying the angular position of one metal rail while keeping the other fixed. On the x-axis, we have the angular position of the movable metal rail, which we were varying for each measurement. In the legend, we can find the angular position of the fixed rail for each graph. Each measurement was taken at a 2-minute interval.

We observe that for each angle of the fixed rail, we reach a maximum number of coincident counts when the movable detector has approximately the same angle ($\theta_s \approx \theta_i$), see Fig. 9. We detect a high number of coincident counts in the scenarios where $\theta_s = \theta_i = 2.5°$, $3°$, and $3.5°$, while for bigger angular positions, the ratio of coincident counts decreases. Therefore, from now on, to conduct the remaining studies, we fix both signal and idler rails at an angle of $\theta_s = \theta_i = 3°$. This agrees with Fig. 9 of [DM02a].

7.3 Optimal angle of the BBO crystals for the production of maximally entangled photons

Once the detectors are placed at the angular position where they detect the highest number of coincidences, our goal is to find the position of the BBO crystals for which the pairs of photons generated by SPDC are maximally entangled. Maximally entangled states are the ones that achieve the maximum violation of the CHSH inequality, making the absolute value of the expected value of S described by Eq. (10) reach its maximum value, $|\langle S \rangle| = 2\sqrt{2}$.

In order to have quantum entanglement at the output of the crystals, we must place them in such a way that the planes $\text{SPDC}_{\text{BBO}_1}$ and $\text{SPDC}_{\text{BBO}_2}$ form an angle of $45°$ with respect to the polarization plane, see Fig. 2 (b). We know that one crystal is rotated $90°$ with respect to the other, thus, the polarization of the photon pairs produced in one crystal is orthogonal to the polarization of the pairs produced in the other crystal. Additionally, for that angle, in both crystals photon pairs are produced with equal probability since the polarization of our pump beam is equally contained in both the $\text{SPDC}_{\text{BBO}_1}$ plane and the $\text{SPDC}_{\text{BBO}_2}$ plane.

To determine the arrangement of the optical axis inside the BBO crystals and thus, know how to place them to produce entangled photon pairs, we rotate the BBO crystals from $0°$ to $360°$ in steps of $10°$. For each of these angles, we take 4 measurements where we vary the orientation of the polarizers placed before the fiber coupler lenses. This al-

lows us to obtain the values of the probabilities $P_{VV}(0°, 0°)$, $P_{HH}(0°, 0°)(P_{VV}(90°, 90°))$, $P_{VH}(0°, 0°)(P_{VV}(0°, 90°))$, and $P_{HV}(0°, 0°)(P_{VV}(90°, 0°))$ for each value of the BBO angle, see Fig. 10.

We shine the BBO crystals with horizontally polarized light as the laser light from the laser is approximately horizontally polarized by default, and we cannot rotate the laser diode once it is fixed inside the temperature-controlled mount [2]. Therefore, if we place the polarizer at the laser output at an angle of 90°, the power loss of the laser beam after passing through the polarizer is minimal. Hence, we can assume that we have the full 40 mW power provided by our diode[3].

To understand what happens in this experiment and calculate the analytical expression of the wavefunction, we can see Fig. 3. Here, we depict a scheme of our procedure in the laboratory to take measurements, where we shine horizontally polarized light onto the BBO crystals, and for different angles (θ) of the crystals, we calculate the probabilities of measuring the pairs of generated photons in the states $|VV\rangle$, $|HH\rangle$, $|VH\rangle$ and $|HV\rangle$.

As we have seen in section 4.1, the wave function corresponding to the photon pairs produced by SPDC as a function of the angle θ of the BBO crystals is given by Eq. (8).

Once we have this wave function, we can proceed to calculate the probabilities of measuring photons in coincidence in the states $|VV\rangle$, $|HH\rangle$, $|VH\rangle$ and $|HV\rangle$, denoted as $P_{VV}(\theta)$, $P_{HH}(\theta)$, $P_{VH}(\theta)$, and $P_{HV}(\theta)$[4].

$$
\begin{aligned}
P_{VV}(\theta) &= |\langle VV|\Psi(\theta)\rangle|^2 = |\cos^3(45°+\theta) - e^{-i\phi(\theta)}\sin^3(45°+\theta)|^2 \\
&= \cos^6(45°+\theta) + \sin^6(45°+\theta) - 2\cos(\phi(\theta))\cos^3(45°+\theta)\sin^3(45°+\theta),
\end{aligned}
$$

$$
\begin{aligned}
P_{HH}(\theta) &= |\langle HH|\Psi(\theta)\rangle|^2 = |\cos(45°+\theta)\sin^2(45°+\theta) - e^{-i\phi(\theta)}\sin(45°+\theta)\cos^2(45°+\theta)|^2 \\
&= \cos^2(45°+\theta)\sin^4(45°+\theta) + \sin^2(45°+\theta)\cos^4(45°+\theta)) - \\
&- 2\cos(\phi(\theta))\cos^3(45°+\theta)\sin^3(45°+\theta),
\end{aligned}
$$

$$
\begin{aligned}
P_{VH}(\theta) &= |\langle VH|\Psi(\theta)\rangle|^2 = |-\cos^2(45°+\theta)\sin(45°+\theta) - e^{-i\phi(\theta)}\sin^2(45°+\theta)\cos(45°+\theta)|^2 \\
&= \cos^4(45°+\theta)\sin^2(45°+\theta) + \sin^4(45°+\theta)\cos^2(45°+\theta)) + \\
&+ 2\cos(\phi(\theta))\cos^3(45°+\theta)\sin^3(45°+\theta),
\end{aligned}
$$

$$
\begin{aligned}
P_{HV}(\theta) &= |\langle HV|\Psi(\theta)\rangle|^2 = |-\cos^2(45°+\theta)\sin(45°+\theta) - e^{-i\phi(\theta)}\sin^2(45°+\theta)\cos(45°+\theta)|^2 \\
&= \cos^4(45°+\theta)\sin^2(45°+\theta) + \sin^4(45°+\theta)\cos^2(45°+\theta)) + \\
&+ 2\cos(\phi(\theta))\cos^3(45°+\theta)\sin^3(45°+\theta).
\end{aligned}
$$

In Fig. 10 we compare these theoretical expressions with our experimental data.

[2] See Annex III for the characterization of the laser polarization.

[3] See Annex IV for the characterization of the laser's optical power.

[4] Remember the change of basis given by Eq. (4)

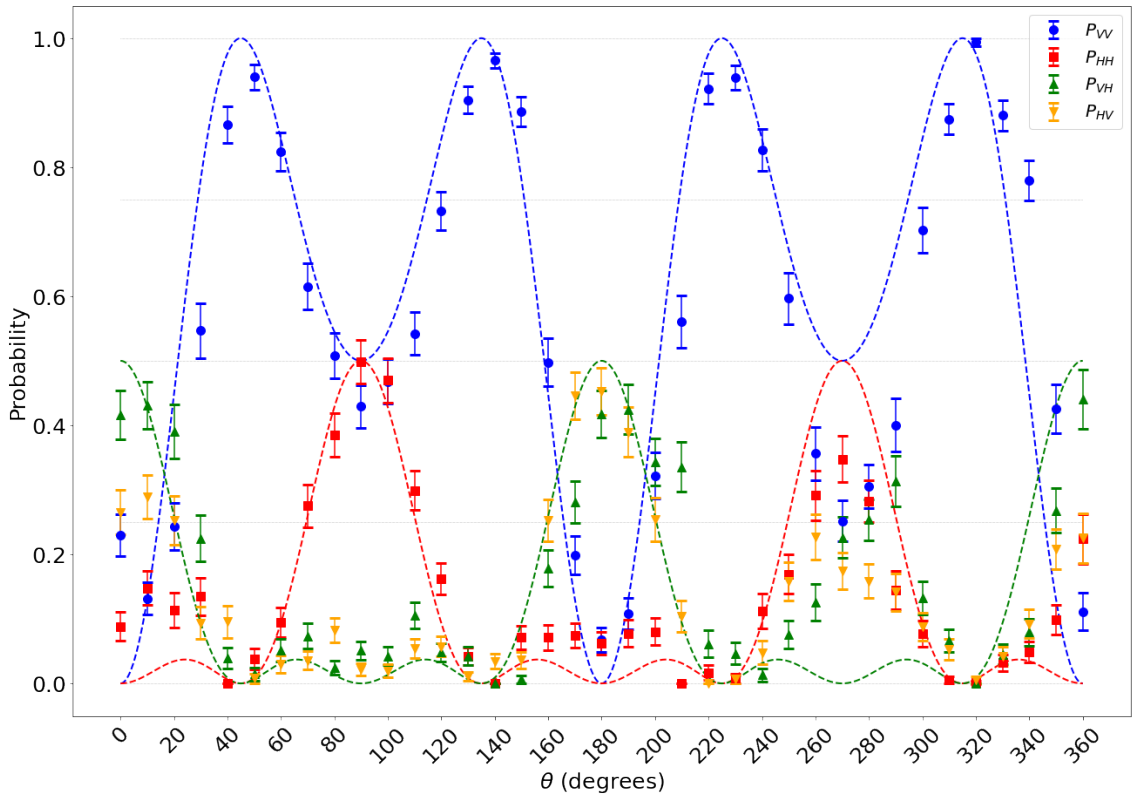

Figure 10: Coincidence probabilities for different angular settings of the BBO crystals and the "signal" and "idler" polarizers. Each measurement is taken over a time interval of 60 seconds. The experimental measurements are the ones graphed with dots (P_{VV}), squares (P_{HH}) and triangles (P_{VH} and P_{HV}) along their statistical error. The theoretical results are plotted with dashed lines.

To plot the theoretical results in Fig. 10, we have assumed a phase difference $\phi(\theta) = 0°$ for all θ. The experimental results follow nicely the predictions of our theoretical model across the entire range of angles, except for the regions from 250° to 300° where we observe that the VH and HV components are larger and the VV and HH components are smaller than what our model predicts and the region from 340° to 380°(20°) where we observe that the VV and HH components are larger and the VH and HV components are smaller than what our model predicts. This discrepancy arises because the assumption of $\phi(\theta) = 0°$ is no longer valid for this interval of angles, causing the terms in the wave function described by Eq. (8) to interfere differently[5].

For angles 45°, 135°, 225°, and 315°, we only have the VV component, see Fig. 10. This gives us an idea of how the optical axis are arranged inside the BBO crystals, both rotated exactly 90° relative to each other and pointing in the directions of 45° and -45°. This is because when we have the crystals oriented at 45°, 135°, 225°, and 315°, only one of the two crystals comes into play producing photon pairs in the state $|VV\rangle$.

[5]See Annex V for a more detailed study of the dependence of the relative phase on the angle θ of the crystals.

This Fig. 10 also shows us the optimal angles of the BBO crystals to achieve a highly entangled state:

- The first one is around 90° because, at these points, we have the HH and VV components of our wave function being predominant and roughly of equal weight, while the HV and VH components are minor and also roughly of equal weight. Furthermore, if we substitute in Eq. (8), assuming $\phi(\theta) = 0°$, we find that at $\theta = 90°$ we have the entangled state

$$|\Psi(\theta = 90°)\rangle = \frac{1}{\sqrt{2}} \left(|VV\rangle + |HH\rangle\right). \tag{12}$$

- The second one is around 180° because, at these points we have the HV and VH components of our wave function being predominant and roughly of equal weight, while the VV and HH components are minor and also roughly of equal weight. As before, if we substitute in Eq. (8), assuming $\phi(\theta) = 0°$, we find that at $\theta = 180°$ we have the entangled state

$$|\Psi(\theta = 180°)\rangle = \frac{1}{\sqrt{2}} \left(|VH\rangle + |HV\rangle\right). \tag{13}$$

- The directions corresponding to 270° and 360° should also generate pairs of entangled photons, similar to the 90° and 180° directions, but we observe that for these directions, the VV, HH, VH, and HV components have similar weights, indicating that the wave function at these points is an equiprobable superposition of the states $|VV\rangle$, $|HH\rangle$, $|VH\rangle$ and $|HV\rangle$. This discrepancy with the theory is possibly due to the fact that for angles of 270° and 360°, the assumption of $\phi(\theta) = 0°$ is no longer valid, and instead, we have $\phi(\theta) \approx 90°$.

8 Entanglement characterization

Once identified the points where we detect a higher number of coincident counts and the angles of the BBO crystals where we expect to find photon pairs in maximally entangled states, we proceed to characterize the entanglement of these photon pairs. First, in Section 8.1, we conduct a study to determine whether the correlation statistics of our photon pairs follow classical or quantum behavior. Second, in Section 8.2, to definitely demonstrate that our photon pairs are in an entangled state by performing the Bell Test.

8.1 Polarization correlations as a function of the polarizers angle difference

One way to determine whether we have quantum or classical correlations is to perform the following experiment. With the BBO crystals set at an angle of 90° and horizontally polarized 405 nm light incident on them, we take different measurements in which for each one we vary the angle of one of the polarizers (e.g. the "signal" polarizer) from 0° to 180° in steps of 10°, while keeping the angle of the other polarizer fixed.

For this system, as we discussed in the previous section, we should expect the BBO crystals to produce pairs of photons in the state

$$|\Psi\rangle = \frac{1}{\sqrt{2}} \left(|VV\rangle + |HH\rangle\right). \tag{14}$$

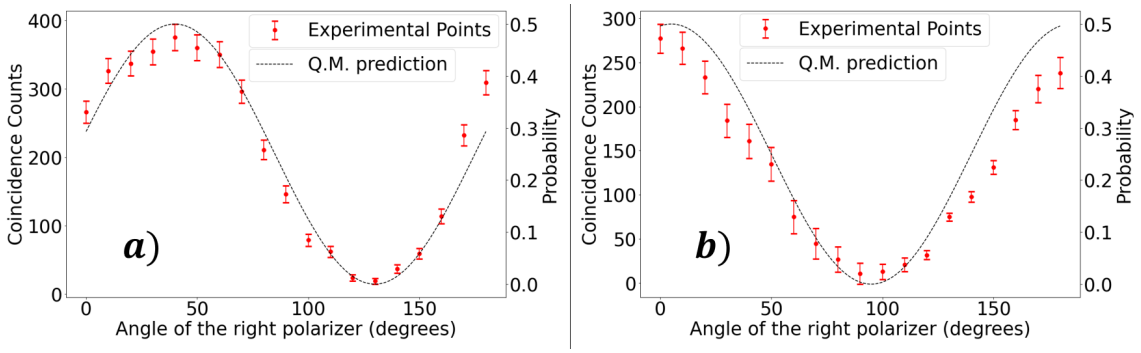

Figure 11: (a) Graph $C(0°, \beta)$. (b) Graph $C(45°, \beta)$. $0°$ and $45°$ are the fixed angles of the left polarizer and β is the variable angle of the right polarizer. Each measurement was taken over a 2-minute interval.

If the coincidence counts follow a dependence like the one observed in Fig. 13 in Annex I, we have that the photon pairs obey the laws of hidden variable theories, whereas if they follow a dependence like the one observed in Fig. 16 in Annex II, we have that the photon pairs obey the laws of quantum mechanics.

In our case, we perform two studies, one where we keep one of the two polarizers fixed at $0°$ and another where we keep it fixed at $45°$, while rotating the other polarizer.

In Fig. 11(a) and Fig. 11(b), we have the experimental data along with their statistical error. We can see that for angles where the polarizers have approximately the same orientation, we obtain a maximum number of coincident counts, while for angles where the polarizers are orthogonal, we obtain a minimum. This also agrees with Fig. 3(a) of [DM02b].

This is further evidence that we are dealing with the state described in Eq. (12), as using the change of basis given by Eq. (4), we can rewrite our wave function as,

$$|\Psi\rangle = \frac{1}{\sqrt{2}} \left(|V\rangle |V\rangle + |H\rangle |H\rangle \right) \longrightarrow \frac{1}{\sqrt{2}} \left(|V_\alpha\rangle |V_\alpha\rangle + |H_\alpha\rangle |H_\alpha\rangle \right),$$

which shows that if we measure one photon to be in a state with polarization along the direction α, we automatically know that the other photon has exactly the same polarization. So with this state, when we measure with both polarizers in the same direction α we obtain a maximum.

8.2 Bell Test

In this last section, we perform the Bell Test for the case where the BBO crystals are placed at an angle $\theta = 90°$ and for the case where they are placed at an angle $\theta = 180°$, illuminating them with horizontally polarized 405 nm light. The wave function of the photon pairs created by SPDC that we expect to find for the first case is given by Eq. (12), while for the second case, it is given by Eq. (13). In both cases, as we will see next, we are able to violate the Bell inequalities using the scenario described by Fig. 6.

8.2.1 Bell Test for $|\Psi(\theta = 90°)\rangle$

α (deg.)	β (deg.)	N_a	N_b	N_c	N_{acc}	$N_c - N_{acc}$		Prob.	Error
-45	-22.5	282677	206976	72	12.18	59.82	P_{VV}	0.314	0.028
-45	22.5	285328	203924	17	12.12	4.88	P_{VV}	0.027	0.012
-45	67.5	285357	203616	32	12.1	19.9	P_{VH}	0.104	0.021
-45	112.5	275012	201176	88	11.52	76.48	P_{VH}	0.415	0.028
0	-22.5	274103	205648	80	11.74	68.26	P_{VV}	0.372	0.028
0	22.5	284537	207284	104	12.28	91.72	P_{VV}	0.446	0.026
0	67.5	284161	206344	46	12.21	33.79	P_{VH}	0.184	0.026
0	112.5	275563	206372	32	11.84	20.16	P_{VH}	0.098	0.020
45	-22.5	272956	211396	43	21.02	21.98	P_{HV}	0.115	0.022
45	22.5	273267	205956	96	11.72	84.28	P_{HV}	0.458	0.027
45	67.5	276790	207824	101	11.98	89.02	P_{HH}	0.467	0.026
45	112.5	267769	206256	30	11.51	18.49	P_{HH}	0.100	0.021
90	-22.5	275212	207640	27	11.9	15.1	P_{HV}	0.082	0.019
90	22.5	280933	208040	26	12.17	13.83	P_{HV}	0.067	0.017
90	67.5	278859	201900	78	11.72	66.28	P_{HH}	0.361	0.028
90	112.5	265509	198720	91	10.99	80.01	P_{HH}	0.389	0.027

Table 1: Collected data used for the computation of S. N_c and N_{acc} denote the number of counts detected in coincidence and the number of accidental coincidence counts, respectively. Each measurement was taken within a time interval of T=120s.

To find the probabilities P that make up each E described in Eq. (9), we need four values of the coincidence counts, each one for different angles of the signal and idler polarizers,

$$P_{VV}(\alpha,\beta) = \frac{N_{VV}(\alpha,\beta)}{N_{tot}(\alpha,\beta)}, \qquad P_{VH}(\alpha,\beta_\perp) = \frac{N_{VV}(\alpha,\beta_\perp)}{N_{tot}(\alpha,\beta)},$$
$$P_{HV}(\alpha_\perp,\beta) = \frac{N_{VV}(\alpha_\perp,\beta)}{N_{tot}(\alpha,\beta)}, \qquad P_{HH}(\alpha_\perp,\beta_\perp) = \frac{N_{VV}(\alpha_\perp,\beta_\perp)}{N_{tot}(\alpha,\beta)},$$

where $N_{tot}(\alpha,\beta) = N_{VV}(\alpha,\beta) + N_{VV}(\alpha,\beta_\perp) + N_{VV}(\alpha_\perp,\beta) + N_{VV}(\alpha_\perp,\beta_\perp)$ is the total number of pairs detected and $\alpha_\perp$, $\beta_\perp$ are the polarizer settings at $\alpha + 90°$ and $\beta + 90°$.

So in order to obtain the four values of E, that is $E(\alpha,\beta)$, $E(\alpha,\beta')$, $E(\alpha',\beta)$ and $E(\alpha',\beta')$ where $\alpha = -45°$, $\alpha' = 0°$, $\beta = -22.5°$ and $\beta' = 22.5°$ we need to compute 16 measurements. The result of each measurement is contained in Table 1. With all these results, we can compute the value for each E along with its error,

$$E(\alpha,\beta) = 0.670 \pm 0.045, \qquad E(\alpha,\beta') = 0.467 \pm 0.052,$$
$$E(\alpha',\beta) = 0.746 \pm 0.043, \qquad E(\alpha',\beta') = -0.561 \pm 0.050.$$

Therefore, the final value of S described by Eq. (10) is:

$$S = 2.443 \pm 0.095.$$

Hence, we can conclude that the wave function describing the state of our photon pairs is entangled, as this result confirms a violation of Bell's inequalities by more than 4 standard deviations.

8.2.2 Bell Test for $|\Psi(\theta = 180°)\rangle$

α (deg.)	β (deg.)	N_a	N_b	N_c	N_{acc}	$N_c - N_{acc}$		Prob.	Error
-45	-22.5	455298	342960	170	16.26	153.74	P_{VV}	0.472	0.020
-45	22.5	403341	326632	51	13.72	37.28	P_{VV}	0.093	0.014
-45	67.5	410081	313788	54	13.4	40.6	P_{VH}	0.125	0.017
-45	112.5	414033	307284	261	13.25	247.75	P_{VH}	0.616	0.015
0	-22.5	369744	258652	64	9.96	54.04	P_{VV}	0.159	0.018
0	22.5	349393	263948	38	9.6	28.4	P_{VV}	0.071	0.012
0	67.5	349936	258452	131	9.42	121.58	P_{VH}	0.358	0.021
0	112.5	413058	292820	213	12.6	200.4	P_{VH}	0.498	0.018
45	-22.5	353674	240344	41	8.85	32.15	P_{HV}	0.099	0.016
45	22.5	322525	232548	110	7.81	102.19	P_{HV}	0.254	0.019
45	67.5	328044	232628	109	9.94	99.06	P_{HH}	0.304	0.021
45	112.5	344015	230004	23	8.24	14.76	P_{HH}	0.037	0.009
90	-22.5	342655	246328	141	8.79	132.21	P_{HV}	0.390	0.021
90	22.5	318821	241340	118	8.01	109.99	P_{HV}	0.273	0.019
90	67.5	329481	245648	40	8.43	31.57	P_{HH}	0.093	0.015
90	112.5	335346	235988	72	8.24	63.76	P_{HH}	0.158	0.017

Table 2: Collected data used for the computation of S. N_c and N_{acc} denote the number of counts detected in coincidence and the number of accidental coincidence counts, respectively. Each measurement was taken within a time interval of T=240s.

Similarly to the previous study, we present the data obtained for the 16 measurements in Table 2. Then, we can compute the value for each E along with its error,

$$E(\alpha,\beta) = -0.542 \pm 0.034, \qquad E(\alpha,\beta') = -0.496 \pm 0.038,$$
$$E(\alpha',\beta) = 0.741 \pm 0.030, \qquad E(\alpha',\beta') = -0.553 \pm 0.038.$$

As a curiosity, we can observe that now $E(\alpha,\beta)$ and $E(\alpha,\beta')$ are negative, while $E(\alpha',\beta)$ is positive. This is because our state is approximately:

$$|\Psi(\theta = 180°)\rangle = \frac{1}{\sqrt{2}}\left(|H_{45°}\rangle\,|H_{45°}\rangle - |V_{45°}\rangle\,|V_{45°}\rangle\right) = \frac{1}{\sqrt{2}}\left(|V\rangle\,|H\rangle + |H\rangle\,|V\rangle\right).$$

Despite this, we can still compute the value of S with our given angles from Fig. 6, by simply readjusting Eq. (10), so that now,

$$S = -E(\alpha,\beta) + E(\alpha',\beta) - E(\alpha,\beta') - E(\alpha',\beta').$$

Thus, we obtain that:

$$S = 2.332 \pm 0.071.$$

Therefore, once again, we can confirm that for this particular angle of the BBO crystals, we are dealing with an entangled state as we manage to violate Bell's inequalities by more than 4 standard deviations.

9 Conclusions

Recalling the objectives we listed in Section 3, we can conclude that we have been able to understand the generation of entangled photon pairs within BBO crystals. This is evidenced by the theoretical development in section 4.1, where we describe the process by which a pump photon generates a photon pair and derive an analytical expression for the wave function of these photon pairs as a function of the BBO crystals angle θ.

We were able to determine how the BBO crystals were arranged, including their optical axes, allowing us to obtain the settings at which maximally entangled states are produced.

Finally, we have managed to demonstrate that for certain configurations of our BBO crystals, the pairs of photons produced are quantum entangled, obtaining a value of S described by Eq. (10) such that $|\langle S \rangle| \geq 2$. Thus, the behave of the pairs of photons produced in our BBO crystals cannot be described using hidden variables theories.

Moving forward, further research is required to understand how the relative phase between components varies with the angle θ of the BBO crystals, thereby achieving a better alignment between the experimental data in Fig. 10 and theoretical predictions. Currently, we already have several theoretical calculations on how this relative phase varies in Annex V.

Our Bell test could in the near future be modified to also close the locality loophole. This can be achieved by separating the two detectors a distance longer than 7.5 meters, i.e. the distance light can travel in 25 ns. In this way, we would ensure that there is no communication possible between the two detectors that could influence their respective measurements.

Bibliography

[ADR82] Alain Aspect, Jean Dalibard, and Gérard Roger. Experimental test of bell's inequalities using time-varying analyzers. *Phys. Rev. Lett.*, 49:1804–1807, Dec 1982.

[AGR82] Alain Aspect, Philippe Grangier, and Gérard Roger. Experimental realization of einstein-podolsky-rosen-bohm gedankenexperiment: A new violation of bell's inequalities. *Phys. Rev. Lett.*, 49:91–94, Jul 1982.

[AJK05] J. B. Altepeter, E. R. Jeffrey, and P. G. Kwiat. Phase-compensated ultra-bright source of entangled photons. *Opt. Express*, 13(22):8951–8959, Oct 2005.

[BB14] Charles H. Bennett and Gilles Brassard. Quantum cryptography: Public key distribution and coin tossing. *Theoretical Computer Science*, 560:7–11, dec 2014.

[BBC+93] Charles H. Bennett, Gilles Brassard, Claude Crépeau, Richard Jozsa, Asher Peres, and William K. Wootters. Teleporting an unknown quantum state via dual classical and einstein-podolsky-rosen channels. *Phys. Rev. Lett.*, 70:1895–1899, Mar 1993.

[Bel64] J. S. Bell. On the Einstein Podolsky Rosen paradox. *Physics Physique Fizika*, 1:195–200, Nov 1964.

[BPM+97] Dik Bouwmeester, Jian-Wei Pan, Klaus Mattle, Manfred Eibl, Harald Weinfurter, and Anton Zeilinger. Experimental quantum teleportation. *Nature*, 390(6660):575–579, 1997.

[BW92] Charles H. Bennett and Stephen J. Wiesner. Communication via one- and two-particle operators on einstein-podolsky-rosen states. *Phys. Rev. Lett.*, 69:2881–2884, Nov 1992.

[CHSH69] John F. Clauser, Michael A. Horne, Abner Shimony, and Richard A. Holt. Proposed experiment to test local hidden-variable theories. *Phys. Rev. Lett.*, 23:880–884, Oct 1969.

[Cou18] Christophe Couteau. Spontaneous parametric down-conversion. *Contemporary Physics*, 59(3):291–304, jul 2018.

[DM02a] Dietrich Dehlinger and MW Mitchell. Entangled photon apparatus for the undergraduate laboratory. *American Journal of Physics*, 70(9):898–902, 2002.

[DM02b] Dietrich Dehlinger and MW Mitchell. Entangled photons, nonlocality, and bell inequalities in the undergraduate laboratory. *American Journal of Physics*, 70(9):903–910, 2002.

[EPR35] A. Einstein, B. Podolsky, and N. Rosen. Can quantum-mechanical description of physical reality be considered complete? *Phys. Rev.*, 47:777–780, May 1935.

[FC72] Stuart J. Freedman and John F. Clauser. Experimental test of local hidden-variable theories. *Phys. Rev. Lett.*, 28:938–941, Apr 1972.

[Jar23] A. Jaramillo. Portable setup for bell test with entangled photons. 2023. Master's Thesis.

[KWW+99] Paul G. Kwiat, Edo Waks, Andrew G. White, Ian Appelbaum, and Philippe H. Eberhard. Ultrabright source of polarization-entangled photons. *Phys. Rev. A*, 60:R773–R776, Aug 1999.

[WJS+98] Gregor Weihs, Thomas Jennewein, Christoph Simon, Harald Weinfurter, and Anton Zeilinger. Violation of bell's inequality under strict einstein locality conditions. *Phys. Rev. Lett.*, 81:5039–5043, Dec 1998.

Annex I: CHSH Bell Test for a HVT model

Hidden variable theories (HVTs) are defined as alternative formulations that assume the existence of certain unknown parameters that would be responsible for the statistical features of quantum mechanics. Such formulations aim to restore the determinism eliminated by the Copenhagen school interpretation, which is the standard interpretation in quantum mechanics.

In our case, as we are working with polarizations and photons, we can think of our HVT as a framework in which each photon has a predefined polarization angle λ, with this angle, we can know beforehand the behavior of each photon. Therefore, when a photon encounters a polarizer that is set at a specific angle γ, it always passes through it (being registered as V_γ) if λ is closer to γ or $\gamma + 180°$ than to $\gamma \pm 90°$; otherwise, the photon stops on it (thus, is registered as H_γ).

We can represent the detector positioned at a certain γ angle as an arrow, see Fig. 12. Thus, the polarization of the photons is given by a lambda angle, which we can also think of as an arrow in this same space. If the polarization arrow falls at an angular distance less than $\frac{\pi}{4}$ or greater than $\frac{3\pi}{4}$ from our polarizer direction, the photon is detected as V_γ and it passes through the polarizer. In any other case, the photon is detected as H_γ and stops at the polarizer. We assume that γ and λ are angles between 0 and 2π. That is, for a detector at a given angle like the one in Fig. 12, if the polarization arrow falls in the green zone, the photon with this polarization passes through the polarizer (V_γ), while if it falls in the red zone, it stops (H_γ).

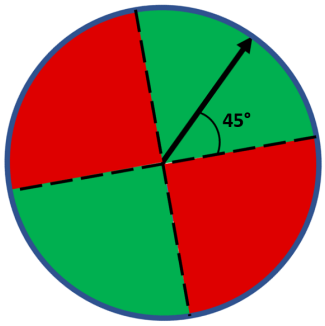

Figure 12: Detection scheme of a polarizer for HVT. Supposing $\gamma > 0°$. The black arrow refers to the direction γ of the polarizer.

We suppose that the signal and idler photon have exactly the same polarization, that is, $\lambda_s = \lambda_i = \lambda$. With this, we try to emulate the wave function,

$$|\Psi\rangle = \frac{1}{\sqrt{2}}(|VV\rangle + |HH\rangle),$$

where if we measure the polarization of one photon in any direction, we are certain that the other photon has the same polarization. As we know, this state can be defined as,

$$|\Psi\rangle = \frac{1}{\sqrt{2}}(|V_\alpha V_\alpha\rangle + |H_\alpha H_\alpha\rangle),$$

using the change of basis described by the system of equations 4.

In each pair of photons, the polarization angle λ changes randomly, spanning the range from 0 to 2π. The variable λ represents the "hidden variable", with this variable we can know beforehand and with certainly the behavior of each photon. Thus, HVTs are:

- *Local*: The outcomes of measurements are influenced by the characteristics of the objects located at the measurement site. The measurement of the signal (idler) photon is determined by the variables λ_s and α (λ_i and β).
- *Realistic*: All observable quantities possess well-defined values. Moreover, the theory precisely specifies these values for a given λ.

So HVTs are *complete* in Einstein's sense of the word, we also say that they are *local realistic* theories. Finally, there is no requirement that λ be random, it is possible that λ change in a deterministic manner yet to be unveiled.

The outcomes of measurements performed on the signal photon are dictated by the function $A(\lambda,\alpha)$, which can produce values of $+1$ when the signal photon is detected as V_α and -1 when is detected as H_α. In a similar way, the outcomes for the idler photon are described by the function $B(\lambda,\beta)$, where $+1$ is obtained when the idler photon is detected as V_β and -1 when is detected as H_β. The functions $A(\lambda,\alpha)$ and $B(\lambda,\beta)$ are defined in Eq. (15).

$$A(\lambda,\alpha)=\begin{cases} 1 \text{ if } |\alpha-\lambda|\leq\frac{\pi}{4} \\ 1 \text{ if } |\alpha-\lambda|>\frac{3\pi}{4} \\ -1 \text{ otherwise}\end{cases}, \qquad B(\lambda,\beta)=\begin{cases} 1 \text{ if } |\beta-\lambda|\leq\frac{\pi}{4} \\ 1 \text{ if } |\beta-\lambda|>\frac{3\pi}{4} \\ -1 \text{ otherwise}\end{cases}, \tag{15}$$

where α (β) is the direction of the signal (idler) polarizer, see [DM02b]. In order to compare this theory with quantum mechanics, it is necessary to make a prediction for the coincidence probability $P^{\text{HVT}}_{\text{VV}}(\alpha,\beta)$. Coincidence takes place when the value of λ falls within a range that is close to both α and β. The probability of such event can be expressed as,

$$P^{\text{HVT}}_{\text{VV}}(\alpha,\beta)=\frac{1}{2\pi}\int_{\lambda=0}^{\lambda=2\pi}\frac{1+A(\lambda,\alpha)}{2}\frac{1+B(\lambda,\beta)}{2}d\lambda=\frac{1}{2}-\frac{|\alpha-\beta|}{\pi}.$$

Note that we are assuming that $0\leq|\alpha-\beta|\leq\frac{\pi}{2}$. Similarly, we can calculate the different probabilities of obtaining VH, HV and HH:

$$P^{\text{HVT}}_{\text{VH}}(\alpha,\beta)=P^{\text{HVT}}_{\text{VV}}(\alpha,\beta+90^\circ)=\frac{1}{2\pi}\int_{\lambda=0}^{\lambda=2\pi}\frac{1+A(\lambda,\alpha)}{2}\frac{1-B(\lambda,\beta)}{2}d\lambda=\frac{|\alpha-\beta|}{\pi},$$

$$P^{\text{HVT}}_{\text{HV}}(\alpha,\beta)=P^{\text{HVT}}_{\text{VV}}(\alpha+90^\circ,\beta)=\frac{1}{2\pi}\int_{\lambda=0}^{\lambda=2\pi}\frac{1-A(\lambda,\alpha)}{2}\frac{1+B(\lambda,\beta)}{2}d\lambda=\frac{|\alpha-\beta|}{\pi},$$

$$P^{\text{HVT}}_{\text{HH}}(\alpha,\beta)=P^{\text{HVT}}_{\text{VV}}(\alpha{+}90^\circ,\beta{+}90^\circ)=\frac{1}{2\pi}\int_{\lambda=0}^{\lambda=2\pi}\frac{1-A(\lambda,\alpha)}{2}\frac{1-B(\lambda,\beta)}{2}d\lambda=\frac{1}{2}-\frac{|\alpha-\beta|}{\pi}.$$

So summarising all these results, we have that:

$$\boxed{\begin{aligned} P^{\text{HVT}}_{\text{HH}}(\alpha,\beta)&=P^{\text{HVT}}_{\text{VV}}(\alpha,\beta)=\frac{1}{2}-\frac{|\alpha-\beta|}{\pi}, \\ P^{\text{HVT}}_{\text{VH}}(\alpha,\beta)&=P^{\text{HVT}}_{\text{HV}}(\alpha,\beta)=\frac{|\alpha-\beta|}{\pi}.\end{aligned}} \tag{16}$$

This probabilities in Eq. (16) are defined in the range $0\leq|\alpha-\beta|\leq\frac{\pi}{2}$. If we calculate and compute these probabilities for $0\leq|\alpha-\beta|\leq2\pi$ we obtain the Fig. 13.

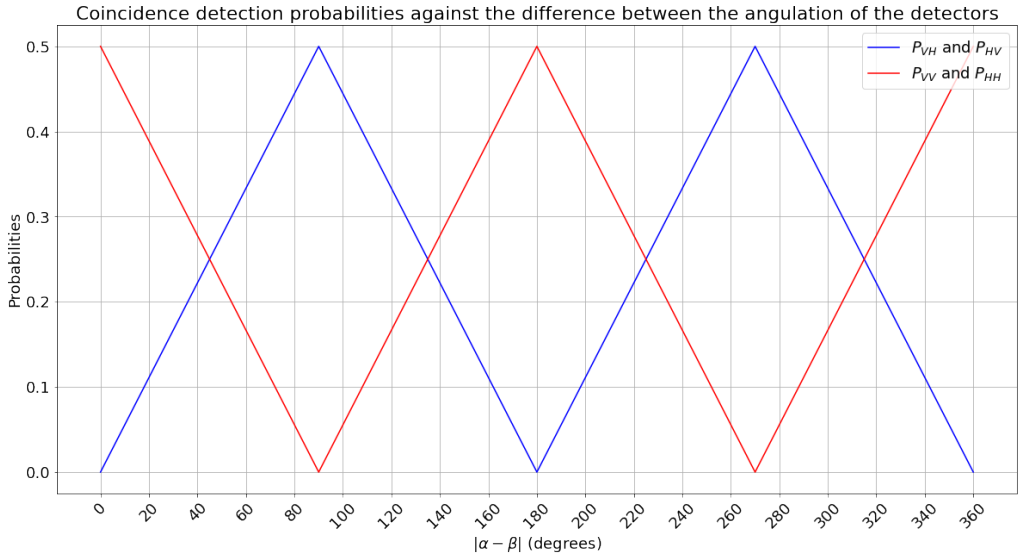

Figure 13: Plot of the different coincidence detection probabilities depending on the difference between the angle of the detectors $|\alpha - \beta|$.

Finally, we can prove that for a HVT model, we cannot violate the CHSH inequality. First of all, lets compute the coincident measurement $E(\vec{a}, \vec{b})$ for any $\vec{a}$ and $\vec{b}$ angles of the signal and idler polarizers,

$$E(\vec{a}, \vec{b}) = \int A(\lambda, \alpha) B(\lambda, \beta) d\lambda \tag{17}$$

In Eq. (9), we introduce the variable s, which characterizes the polarization correlations in a single pair of particles.

$$\begin{aligned} s &= A(\lambda, \alpha)B(\lambda, \beta) + A(\lambda, \alpha')B(\lambda, \beta) + A(\lambda, \alpha)B(\lambda, \beta') - A(\lambda, \alpha')B(\lambda, \beta') \\ &= A(\lambda, \alpha)[B(\lambda, \beta) + B(\lambda, \beta')] + A(\lambda, \alpha')[B(\lambda, \beta) - B(\lambda, \beta')]. \end{aligned}$$

where α, α', β, β' are the angles depicted in Fig. 6. The variable s is restricted to the values of ± 2, as $A(\lambda, \alpha)$ and $B(\lambda, \beta)$ can only take the values ± 1. Therefore, the average value S must fall within the range of $-2 \leq S \leq +2$. Thus, the value of $|\langle S \rangle| = 2$ is not surpassed for any configuration of the polarizers ($\vec{a}$, $\vec{a'}$, $\vec{b}$, $\vec{b'}$) and any photon polarization λ.

To help us in the visualization and interpretation of the Hidden Variable Theory, we now present two simple examples. One in which both polarizers have the same angle ($|\alpha - \beta| = 0$), and another in which they do not have the same angle ($|\alpha - \beta| \neq 0$).

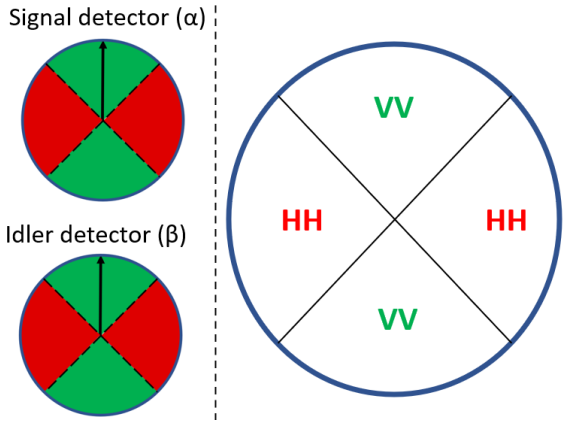

Figure 14: Coincidence detection scheme for $\vec{a} = \vec{b}$

In this Fig. 14 we can see the directions of both polarizers on the left, as well as a big wheel which represents the measurement we obtain if a certain polarization given by a vector $\vec{\lambda}$ falls in one of these four triangles. We can see that the two triangles VV occupy the same (25% of the wheel each), and the same is true for the two triangles HH. Therefore, if we distribute evenly on this wheel different polarizations $\vec{\lambda}$, we have a 50% probability of measuring VV and a 50% probability of measuring HH, while we have a 0% probability of measuring HV or VH. This can be checked with the formulas presented in the box above, Eq. (16).

Also, we can represent a more generical scheme of coincidence detection, when $\vec{a} \neq \vec{b}$, it is when the signal and idler detectors do not point in the same direction.

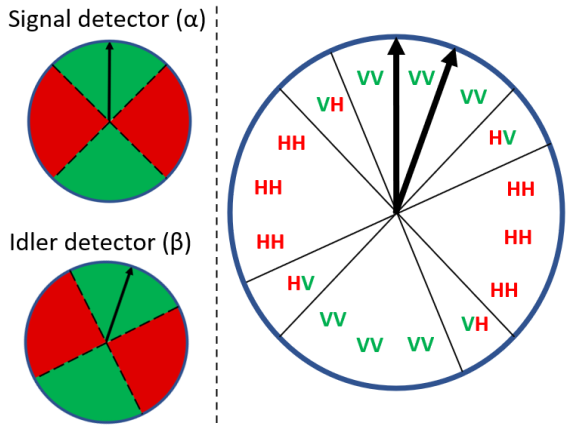

Figure 15: Coincidence detection scheme for $\vec{a} \neq \vec{b}$

In this Fig. 15 we have a more complicated scenario. The big wheel represents all the possible measurement outcomes for a given polarization $\vec{\lambda}$ and the big black arrows represent the directions of the signal and idler polarizers. The first letter inside each triangle in the wheel is the measurement outcome related to the signal party while the second letter is the measurement outcome related to the idler party. We can see that in this scenario we have a nonzero probability of obtain HV or VH, and both with the same probability because their corresponding triangles occupy the same area in the wheel. The same occurs for the coincidence detection of VV and HH.

Annex II: CHSH Bell Test for a QM model

Since the state we want to reproduce in the laboratory is,

$$|\Psi_{EPR}\rangle = \frac{1}{\sqrt{2}}\left(|V\rangle_s |V\rangle_i + |H\rangle_s |H\rangle_i\right), \tag{18}$$

where $|V\rangle$ and $|H\rangle$ indicate vertical and horizontal polarizations respectively, and the subscripts indicate signal (s) or idler (i) photon. If we measure the polarizations of signal and idler photons in the H, V basis, there are only two possible outcomes: both having vertical polarization or both having horizontal polarization and each outcome occurs half of the time. Alternatively, we can conduct measurements of the polarization by employing polarizers that are rotated at an angle α. Then we use the rotated polarization basis:

$$\begin{cases} |V_\alpha\rangle = \cos(\alpha)|V\rangle - \sin(\alpha)|H\rangle \\ |H_\alpha\rangle = \sin(\alpha)|V\rangle + \cos(\alpha)|H\rangle \end{cases}. \tag{19}$$

It is easy to find out that,

$$|\Psi_{EPR}\rangle = \frac{1}{\sqrt{2}}\left(|V_\alpha\rangle_s |V_\alpha\rangle_i + |H_\alpha\rangle_s |H_\alpha\rangle_i\right). \tag{20}$$

This Eq. (20) is very important as it shows that the vertical and horizontal directions can be chosen arbitrarily, assuming that these two directions are perpendicular to each other, when we have the state described in Eq. (18). In this state, if the signal photon is measured using a polarizer at an angle α, the outcome will be either H_α or V_α, where each possibility is equally likely, the same applies to the idler photon.

$$|\langle\Psi_{EPR}|\left(|V_\alpha\rangle_s \otimes \mathbb{I}_i\right)|^2 = 1/2 \qquad \text{and} \qquad |\langle\Psi_{EPR}|\left(|H_\alpha\rangle_s \otimes \mathbb{I}_i\right)|^2 = 1/2.$$

Thus, when the photons go through their respective polarizers, we cannot determine with total certainty whether they pass through their polarizers or not (as we did in the hidden variable theory), we can only obtain the probability of each possible scenario, which depends on the difference between the angles α and β of the polarizers. That is:

$$|\Psi_{EPR}\rangle \longrightarrow \begin{cases} P_{V_{\alpha_i}} = \frac{1}{2} \longrightarrow \begin{cases} P_{V_{\beta_i}|V_{\alpha_i}} = |\langle V_\alpha|V_\beta\rangle_i|^2 = \cos^2(\alpha-\beta) \\ P_{H_{\beta_i}|V_{\alpha_i}} = |\langle V_\alpha|H_\beta\rangle_i|^2 = \sin^2(\alpha-\beta) \end{cases} \\ P_{H_{\alpha_i}} = \frac{1}{2} \longrightarrow \begin{cases} P_{V_{\beta_i}|H_{\alpha_i}} = |\langle H_\alpha|V_\beta\rangle_i|^2 = \sin^2(\alpha-\beta) \\ P_{H_{\beta_i}|H_{\alpha_i}} = |\langle H_\alpha|H_\beta\rangle_i|^2 = \cos^2(\alpha-\beta) \end{cases} \end{cases}$$

Summarising all these results, we have,

$$\boxed{\begin{aligned} P_{HH}^{QM}(\alpha,\beta) &= P_{VV}^{QM}(\alpha,\beta) = \frac{1}{2}\cos^2(\alpha-\beta), \\ P_{VH}^{QM}(\alpha,\beta) &= P_{HV}^{QM}(\alpha,\beta) = \frac{1}{2}\sin^2(\alpha-\beta). \end{aligned}} \tag{21}$$

Plotting these results in the same way as for the HVT case:

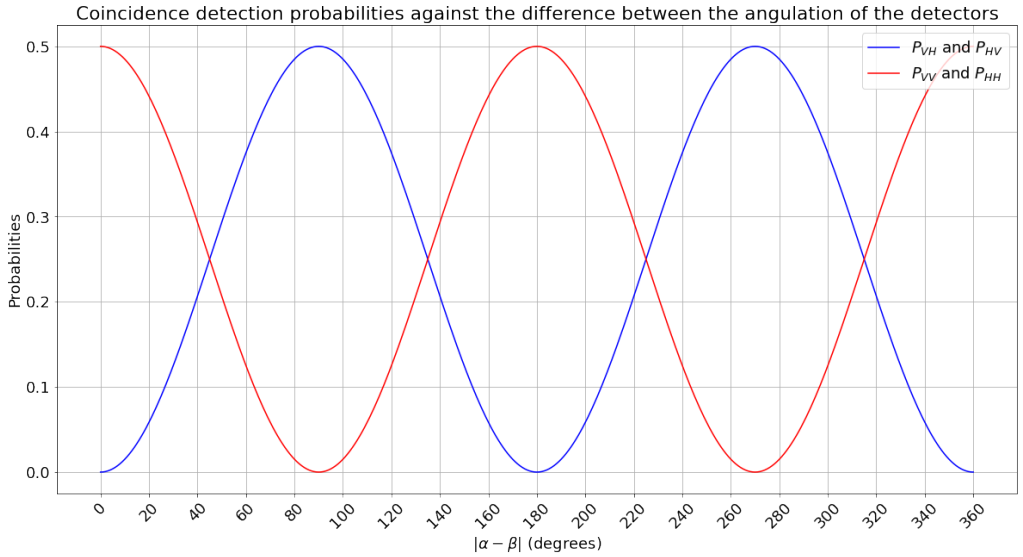

Figure 16: Plot of the different coincidence detection probabilities depending on the difference between the angle of the detectors $|\alpha-\beta|$.

With the probabilities shown in Eq. (21) we can calculate the value of E (see Eq. (9)) for each values of the polarizers angle,

$$\begin{aligned} E(\vec{a},\vec{b}) &= P_{VV}(\vec{a},\vec{b}) + P_{VH}(\vec{a},\vec{b}) + P_{HV}(\vec{a},\vec{b}) + P_{HH}(\vec{a},\vec{b}) = \cos(2(\alpha-\beta)), \\ E(\vec{a'},\vec{b}) &= P_{VV}(\vec{a'},\vec{b}) + P_{VH}(\vec{a'},\vec{b}) + P_{HV}(\vec{a'},\vec{b}) + P_{HH}(\vec{a'},\vec{b}) = \cos(2(\alpha'-\beta)), \\ E(\vec{a},\vec{b'}) &= P_{VV}(\vec{a},\vec{b'}) + P_{VH}(\vec{a},\vec{b'}) + P_{HV}(\vec{a},\vec{b'}) + P_{HH}(\vec{a},\vec{b'}) = \cos(2(\alpha-\beta')), \\ E(\vec{a},\vec{b}) &= P_{VV}(\vec{a'},\vec{b'}) + P_{VH}(\vec{a'},\vec{b'}) + P_{HV}(\vec{a'},\vec{b'}) + P_{HH}(\vec{a'},\vec{b'}) = \cos(2(\alpha'-\beta')). \end{aligned}$$

Then, taking the set of angles of the Fig. 6, that is $(\alpha-\beta) = 22.5°$, $(\alpha-\beta') = -22.5°$, $(\alpha'-\beta) = -22.5°$ and $(\alpha'-\beta') = -67.5°$, we can compute the expectation value of S, given by Eq. (10),

$$\langle S\rangle = E(\vec{a},\vec{b}) + E(\vec{a'},\vec{b}) + E(\vec{a},\vec{b'}) - E(\vec{a'},\vec{b'}) = \frac{1}{\sqrt{2}} + \frac{1}{\sqrt{2}} + \frac{1}{\sqrt{2}} - \left(\frac{-1}{\sqrt{2}}\right) = 2\sqrt{2}.$$

This result $\langle S\rangle = 2\sqrt{2}$ corresponds to the maximum violation of Bell's inequalities for a theory that follows the rules of quantum mechanics.

The fact that Bell's inequalities are violated has two very important implications:

- **Non-locality:** The violation of Bell's inequalities shows that entangled quantum systems can exhibit correlations that cannot be explained by local theories. This implies that quantum information can propagate instantaneously over large distances, challenging the principle of locality in classical physics.
- **Rejection of hidden local theories:** Bell's inequalities are derived from assumptions of local realism, which imply that the physical properties of objects exist independently of observation and that these properties can be determined locally. The violation of these inequalities shows that hidden local theories, which attempt to explain quantum results through pre-existing hidden variables, are inconsistent with quantum physics.

Annex III: Malus' Law of the Laser Polarizer

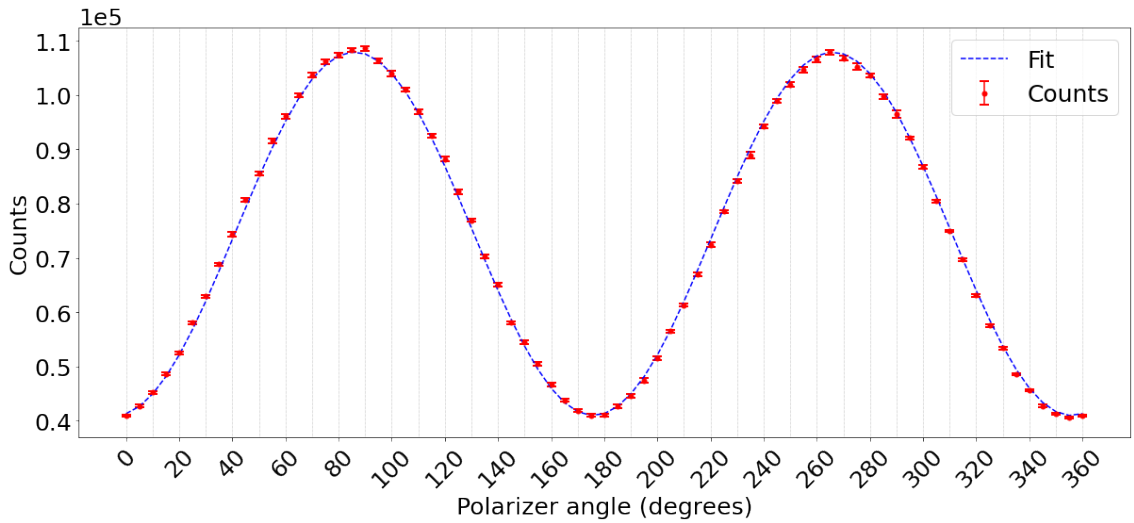

Figure 17: Number of counts along with their statistical error received on average every 0.5 seconds in the detector as a function of the polarizer angle (red points). Also, a fit of the experimental graph to a sine-square function is included (blue dashed line)

To verify that the operation of all components was as expected, some studies were carried out. First, we checked that the polarizer placed in the laser mount follows Malus' law. To carry out this study, we aligned one of the detectors so that it collected the highest number of 405 nm photons at the laser output. Then, while working with the laser at the minimum power to avoid damaging or saturating the detectors, we varied the angle of the polarizer from 0° to 360° in steps of 5°. The detector gave us a reading of the number of counts received every half second and for each angle. The total data acquisition time was 30 seconds, so a total of 60 data were averaged for each measurement.

In Fig. 17 we have made a fit to a function of the form,

$$f(x, a, b, c) = a \cdot \sin^2 \theta + c, \qquad \text{where} \qquad \theta = \frac{(x + b) \cdot \pi}{180}.$$

Obtaining the following values of the three variables,

$$a = 66989.51 \pm 245.00,$$
$$b = 4.11 \pm 0.11,$$
$$c = 40945.85 \pm 149.00.$$

These results reveal that the light initially comes out of the laser forming an angle of 94.11° with the vertical[6]. Since the experimental results follow properly the Law of Malus, we can conclude that the polarizer at the output of the laser works correctly and that the 405 nm light from the diode is linearly polarized.

[6]Taking counterclockwise direction as positive when we observe the light propagating away from us

Annex IV: Optical Power Laser Diode

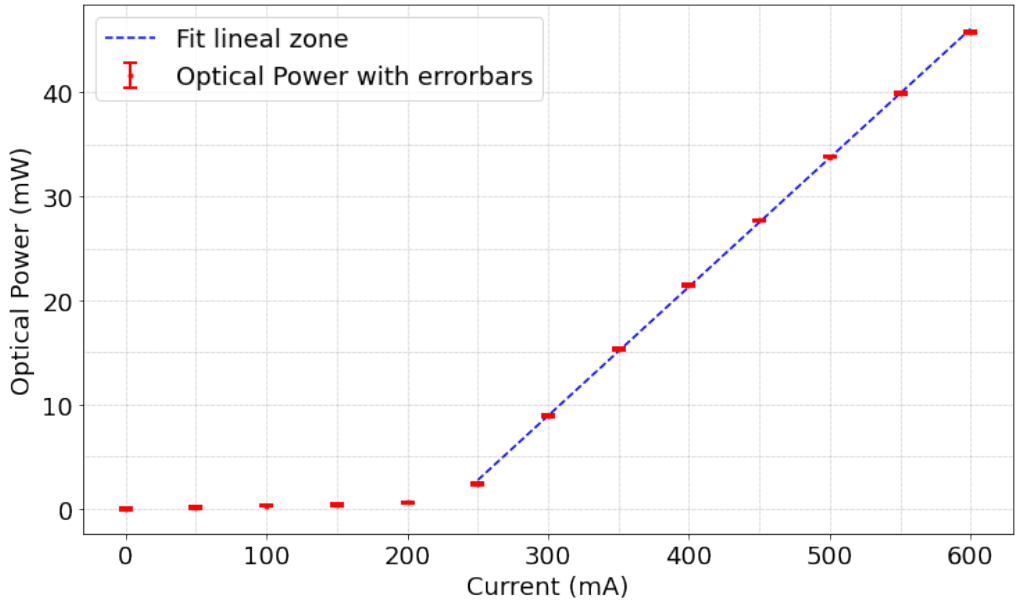

Figure 18: Characteristic curve of laser diode emission. A linear fit has been performed on the data points within the stimulated emission zone.

To observe the dependence of the optical power of our laser diode on the current passing through it, we used a calibrated potentiometer at 405 nm, which we placed right at the laser output. For the generation of the emission curve, we varied the current passing through the laser diode from 0 mA to 600 mA in 50 mA increments. For each of these currents, we recorded the corresponding optical power value indicated by the potentiometer, see Fig. 18.

Firstly, we observe the zone corresponding to spontaneous emission, which ranges from approximately 0 mA to 200 mA, see Fig. 18. When the diode operates in this zone, we have a broad frequency spectrum and a non-coherent emission because photons are randomly emitted and not synchronized in phase or frequency.

On the other hand, we can observe the zone of stimulated emission of the laser, which ranges from 250 mA to 600 mA, the maximum current at which our laser can operate, see Fig. 18. At this current, we achieve optical power values of 45.8 mW [7]. This zone is characterized by coherent laser emission and a narrow emission spectrum. Performing a linear fit to these points, we obtain the following values for the slope, intercept, and their respective errors,

$$m = 0.124 \pm 0.001 \ mW/mA,$$
$$n = -28.257 \pm 0.308 \ mW.$$

Where m is the slope and n is the intercept. With these values, we can determine the threshold current of our laser diode, which is the point at which our linear fit intersects the x-axis. Thus, we obtain that the threshold current is 228.1 ± 2.8 mA.

[7] We work with power levels around 40 mW to avoid damaging the laser diode

Annex V: Relative Phase dependence with θ

A theoretical development has been carried out to know how the phase between components of our wave function varies as a function of the BBO's angle θ in the case where a pump photon passes through a pair of BBO crystals, undergoing SPDC in the process, and resulting in a pair of photons at the output. The study has been conducted for two cases:

- One where the BBO crystals are perfectly aligned, with the face upon which the pump photons hit being perpendicular to their propagation direction.
- Another study where BBO crystals are slightly tilted and the face upon which the pump photons hit is not perpendicular to their propagation direction.

In both cases, pump photons that suffer SPDC inside a BBO crystal are extraordinary-polarized and downconvert into two photons with ordinary-polarized. Then, as one BBO crystal is rotated 90° with respect to the other, photons extraordinary-polarized in one BBO crystal are ordinary-polarized in the other crystal and vice versa. Before starting with the study, we make some assumptions:

- SPDC is produced in the center of each BBO crystal.
- The "signal" and "idler" photons travel in completely symmetrical directions with respect to the pump beam

Relative Phase Depende: Perfect alignment of the crystals

First, we will see what happens inside the BBO crystals in the detection plane of our experiment. The detection plane is the plane that contains both the 405 nm laser beam after reflection in the second crystal and all the detection elements, see Fig. 8. For this, we rely on Fig. 19.

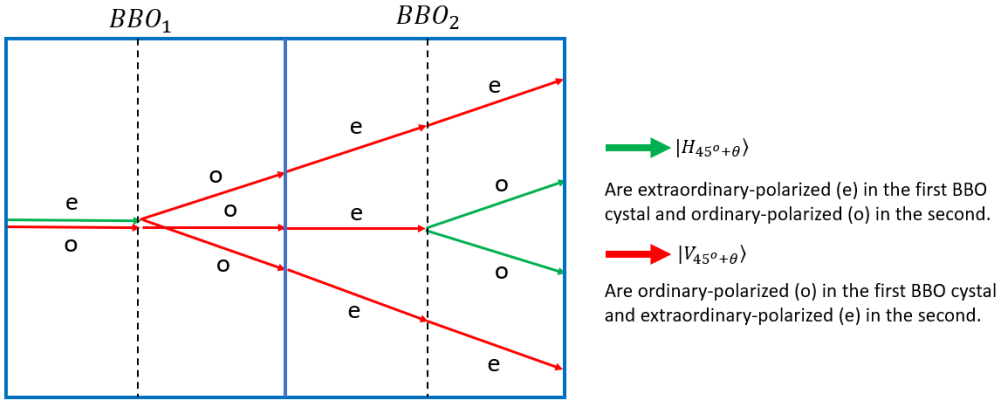

Figure 19: Optical path scheme followed by photons that suffer SPDC when passing through the BBO crystals. The BBO crystals in this illustration are cut by the detection plane (see Fig. 8).

- In the first stage, from the moment the pump photon strikes on the BBO crystals until SPDC occurs in the first crystal, we have that the $|H_{45^\circ+\theta}\rangle$ component of the pump photons propagates with effective velocity, while the $|V_{45^\circ+\theta}\rangle$ component of the pump photons propagates with ordinary velocity.

- In the second stage, from the moment the SPDC occurs in the first crystal until the photons reach the second crystal, we have that the $|V_{45°+\theta}\rangle_s |V_{45°+\theta}\rangle_i$ component of the downconvert photons propagates with ordinary velocity and forming an angle of approximately 3° with respect to the pump beam, while the $|V_{45°+\theta}\rangle$ component of the pump photons continues propagating with ordinary velocity.

- In the second stage, from the moment the photons reach the second crystal until SPDC occurs in the second crystal, we have that the $|V_{45°+\theta}\rangle_s |V_{45°+\theta}\rangle_i$ component of the downconvert photons propagates with effective velocity and forming an angle of approximately 3° with respect to the pump beam, while the $|V_{45°+\theta}\rangle$ component of the pump photons propagates also with effective velocity.

- In the third stage, from the moment the SPDC occurs in the second crystal until the photons exit from the second crystal, we have that the $|V_{45°+\theta}\rangle_s |V_{45°+\theta}\rangle_i$ component of the downconvert photons propagates with effective velocity and forming an angle of approximately 3° with respect to the pump beam, while the $|H_{45°+\theta}\rangle_s |H_{45°+\theta}\rangle_i$ component of the downconvert photons propagates with ordinary velocity and forming an angle of approximately 3° with respect to the pump beam.

The effective velocity at which extraordinarily polarized photons propagate varies depending on the angle between the optical axis and their propagation direction. Thus, the effective refractive index experienced by an extraordinarily polarized beam propagating at an angle α with respect to the optical axis is:

$$n^{\text{eff}}(\alpha) = \sqrt{\frac{1}{\frac{\cos^2\alpha}{n_e^2} + \frac{\sin^2\alpha}{n_o^2}}} \tag{22}$$

In Fig. 20, we can see the propagation directions of the photons, the direction of the optical axis and the arrangement of the different planes of interest inside a BBO crystal.

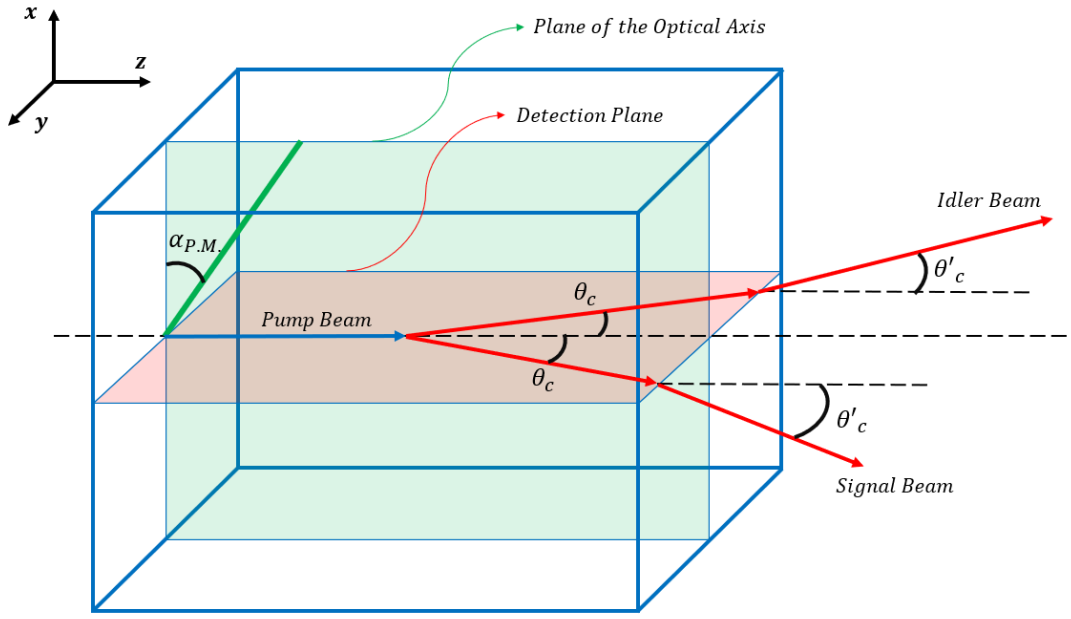

Figure 20: View of the propagation directions of the photons, the direction of the optical axis and the arrangement of the different planes of interest inside a BBO crystal.

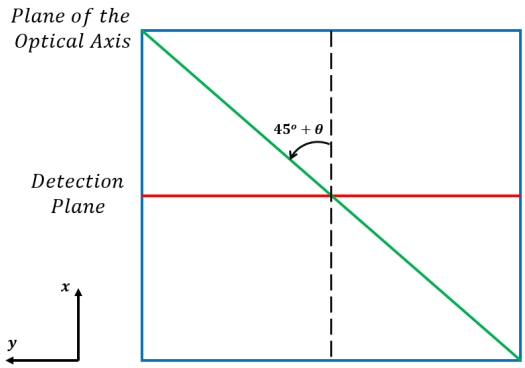

Figure 21: Front view of the second BBO crystal.

When the pair of photons generated in the first crystal pass through the second crystal, the scenario is different because now these photons have polarization contained in the plane of the optical axis, see Fig. 19. If we denote $\alpha_s(\theta)$ ($\alpha_i(\theta)$) as the angle formed by the propagation direction of the signal (idler) photons with the optical axis, in the second crystal, the signal and idler photons propagate with an effective refractive index of $n^{\text{eff}}(\alpha_s(\theta))$ and $n^{\text{eff}}(\alpha_i(\theta))$, respectively.

If we observe the second crystal from the front, we have that for $\theta = 0°$, the plane of the optical axis and the detection plane form an angle of 45°, see Fig. 21.

Next, knowing how the different planes of interest are arranged and what are the propagation directions of the photons inside our second BBO crystal, we proceed to calculate the analytical expression for the angles $\alpha_s(\theta)$ and $\alpha_i(\theta)$ as a function of the crystal rotation angle (and thus, the rotation angle of the plane of the optical axis). To do this, we rely on Fig. 22.

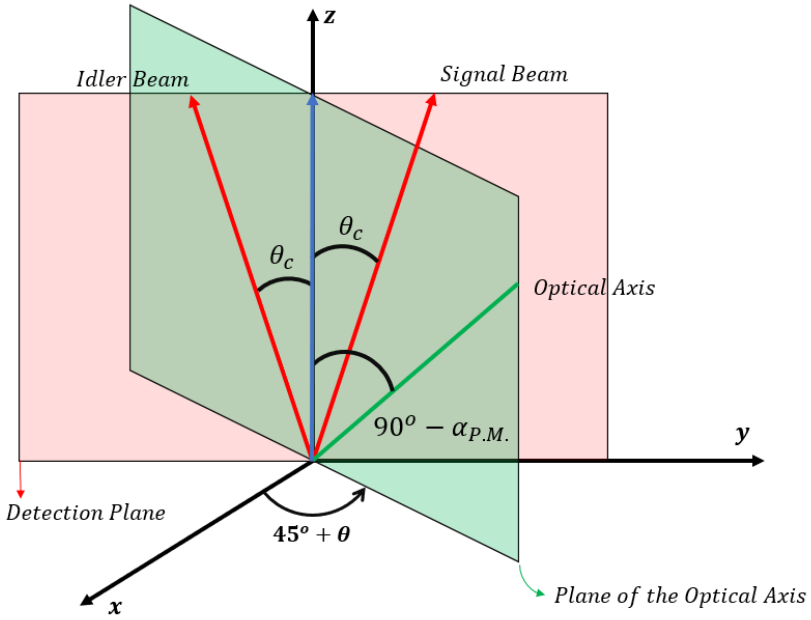

Figure 22: Diagram illustrating the arrangement of planes and the propagation directions of the photons produced by SPDC in the first crystal inside the second BBO crystal.

If we compute the vectors that point in the propagation directions of the signal and idler photons ($\hat{s}$ and $\hat{i}$ respectively) and the vector that point in the direction of the optical axis ($\hat{o}$) as a function of the rotation angle θ:

$$\begin{aligned}
\hat{s} &= (0, \sin\theta_c, \cos\theta_c)\,, \\
\hat{i} &= (0, -\sin\theta_c, \cos\theta_c)\,, \\
\hat{o} &= (\cos\alpha_{P.M.} \cdot \cos(45^\circ + \theta), \cos\alpha_{P.M.} \cdot \sin(45^\circ + \theta), \sin\alpha_{P.M.})\,,
\end{aligned}$$

then we have that $\alpha_s(\theta)$ and $\alpha_i(\theta)$ are:

$$\begin{aligned}
\cos(\alpha_s(\theta)) = \hat{s}\cdot\hat{o} \longrightarrow \alpha_s(\theta) = \arccos(\cos\theta_c \cdot \sin\alpha_{P.M.} + \sin\theta_c \cdot \cos\alpha_{P.M.} \cdot \sin(45^\circ + \theta)), \\
\cos(\alpha_i(\theta)) = \hat{i}\cdot\hat{o} \longrightarrow \alpha_i(\theta) = \arccos(\cos\theta_c \cdot \sin\alpha_{P.M.} - \sin\theta_c \cdot \cos\alpha_{P.M.} \cdot \sin(45^\circ + \theta)).
\end{aligned}$$

Now, we can compute the relative phase introduced in the wave function as,

$$\begin{aligned}
\phi = \phi_1 + \phi_2 + \phi_3 + \phi_4 =& 2\pi\frac{d}{4}\left[\frac{1}{\lambda}\left(n^{\text{eff}}(\alpha_{P.M.}) - n_o\right) + \left(\frac{1}{\lambda'}\cdot\frac{2}{\cos\theta_c} - \frac{1}{\lambda}\right)\cdot n_o + \right. \\
&+ \left(\frac{1}{\lambda'}\cdot\frac{n^{\text{eff}}(\alpha_s(\theta)) + n^{\text{eff}}(\alpha_i(\theta))}{\cos\theta_c} - \frac{1}{\lambda}\cdot n^{\text{eff}}(\alpha_{P.M.})\right) \\
&\left. + \left(\frac{1}{\lambda'}\cdot\frac{n^{\text{eff}}(\alpha_s(\theta)) + n^{\text{eff}}(\alpha_i(\theta))}{\cos\theta_c} - \frac{1}{\lambda'}\cdot\frac{2}{\cos\theta_c}\cdot n_o\right)\right] = \\
=& 2\pi\frac{d}{4}\left[\frac{-2}{\lambda}\cdot n_o + \frac{2}{\lambda'}\cdot\frac{n^{\text{eff}}(\alpha_s(\theta)) + n^{\text{eff}}(\alpha_i(\theta))}{\cos\theta_c}\right].
\end{aligned}$$

So:

$$\boxed{\phi(\theta) = 2\pi\frac{d}{4}\left[\frac{-2}{\lambda}\cdot n_o + \frac{2}{\lambda'}\cdot\frac{n^{\text{eff}}(\alpha_s(\theta)) + n^{\text{eff}}(\alpha_i(\theta))}{\cos\theta_c}\right].} \tag{23}$$

Where d is the total thickness of both crystals. For our case, the values we take for all the different variables involved in the study are:

$$\boxed{\begin{aligned}
&\theta_c = 2^\circ, \\
&\alpha_{P.M.} = 29.2^\circ, \\
&n_e = 1.655, \\
&n_o = 1.542, \\
&d = 0.2 \text{ mm}, \\
&\lambda = 405 \text{ nm}, \\
&\lambda' = 810 \text{ nm}.
\end{aligned}} \tag{24}$$

With all of this, we can plot the dependence of the angles $\alpha_s(\theta)$ and $\alpha_i(\theta)$ as a function of θ, see Fig. 23, as well as the effective refractive index that the photons would experience, i.e., $n^{\text{eff}}(\alpha_s(\theta))$ and $n^{\text{eff}}(\alpha_i(\theta))$, see Fig. 24.

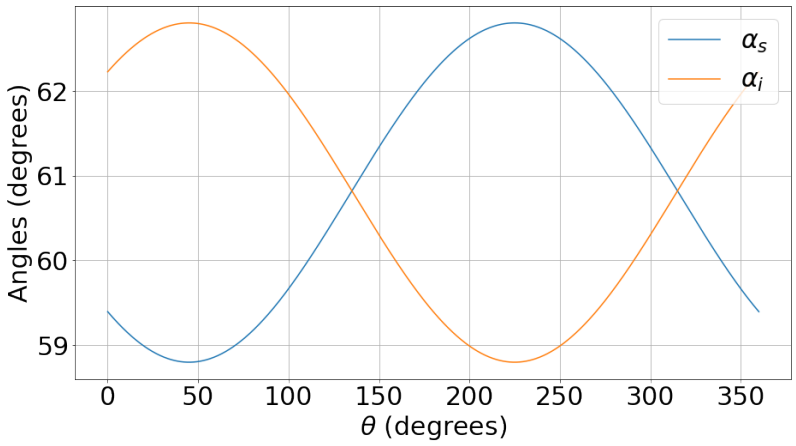

Figure 23: Angle formed by the propagation directions of the signal and idler photons generated in the first crystal with the optical axis of the second crystal as a function of the rotation angle of the BBO crystals.

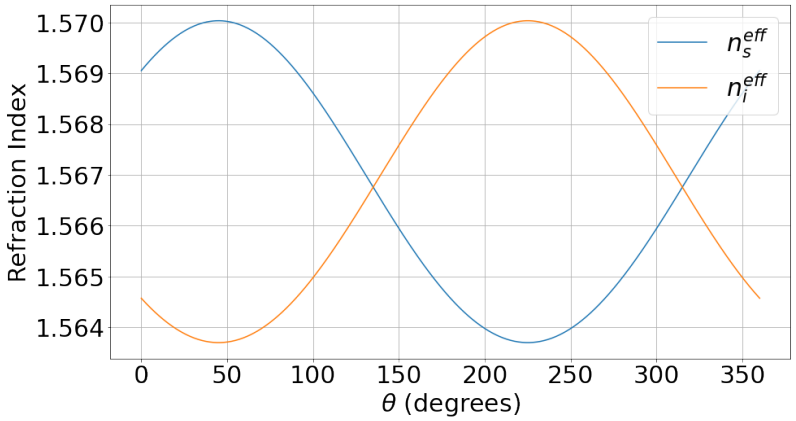

Figure 24: Effective refractive index of the signal and idler photons generated in the first crystal as a function of the rotation angle of the BBO crystals.

With all of this, the relative phase introduced as a function of the crystal angle is shown in Fig. 25.

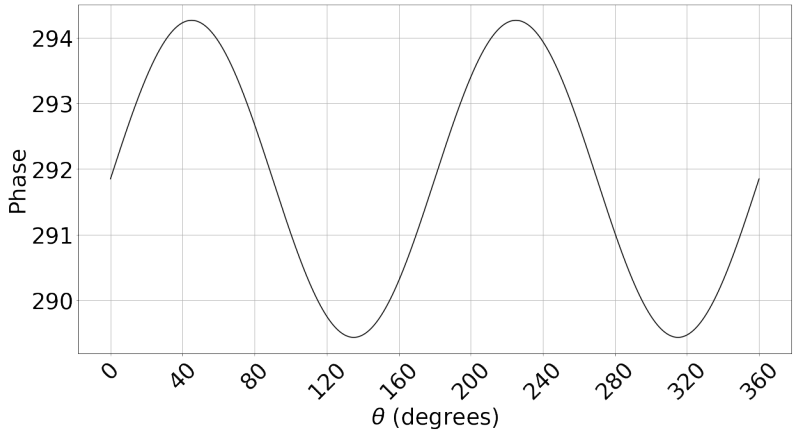

Figure 25: Relative phase between components as a function of the rotation angle of the BBO crystals.

Fig. 25 shows that the phase difference between the maximum and minimum point is only 4 degrees, so if the BBO crystals are perfectly aligned in our setup, the relative phase introduced between the components when rotating the BBO crystals is approximately the same at all angles.

Relative Phase Depende: BBO crystals slightly tilted

Now, we assume that the BBO crystals are not perfectly aligned but are tilted by a small angle γ. A scheme of what we observe if we cut the BBO crystals along the detection plane is depicted in Fig. 26.

Note that now the refractive index also varies with the angle for the pump photons propagating with extraordinary polarization in both the first and second BBO crystals. That is why we now have two new angles, $\alpha_p^1(\theta)$ and $\alpha_p^2(\theta)$, where $\alpha_p^1(\theta)$ ($\alpha_p^2(\theta)$) is the angle formed between the propagation direction of the pump photons with extraordinary polarization and the optical axis of the first (second) BBO crystal.

Just like in the previous section, to calculate the angles $\alpha_s(\theta)$, $\alpha_i(\theta)$, $\alpha_p^1(\theta)$ and $\alpha_p^2(\theta)$, we rely on Fig. 27(a) and on Fig. 27(b).

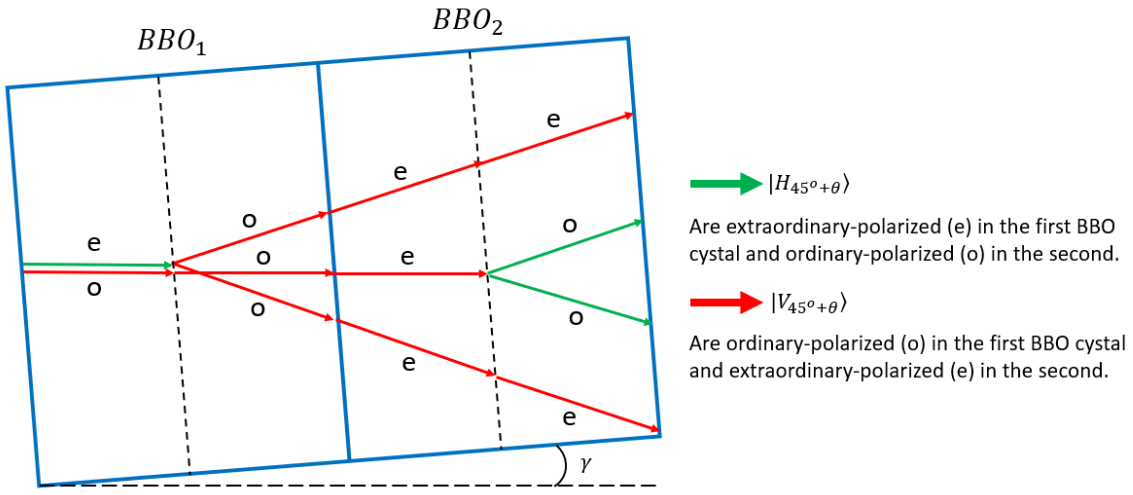

Figure 26: Optical path scheme followed by photons that suffer SPDC when passing through the BBO crystals.

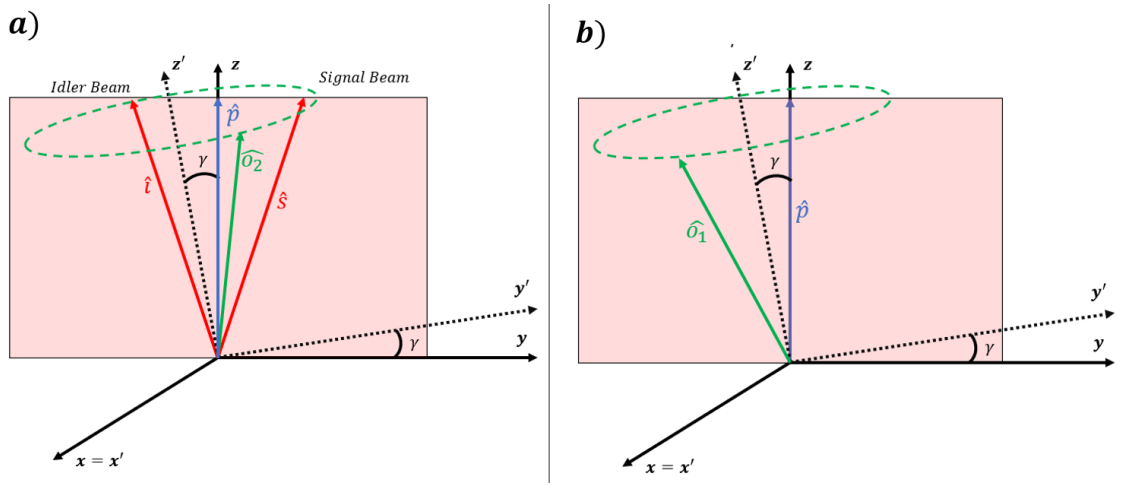

Figure 27: (a) Arrangement of the detection plane, the propagation direction of the pump photons ($\hat{p}$) and the direction of the optical axis ($\hat{o_1}$) inside the first BBO crystal. (b) Arrangement of the detection plane, the propagation direction of the pump photons ($\hat{p}$), the propagation direction of the signal and idler photons ($\hat{s}$ and $\hat{i}$) and the direction of the optical axis ($\hat{o_2}$) inside the second BBO crystal.

If we compute the vectors that point in the propagation directions of the pump photons ($\hat{p}$), the signal and idler photons ($\hat{s}$ and $\hat{i}$ respectively) and the vectors that point in the directions of the optical axis ($\hat{o_1}$ and $\hat{o_2}$) as a function of the rotation angle θ in the (x', y', z') basis:

$$
\begin{aligned}
\hat{p} &= (0, \sin(\gamma), \cos(\gamma))\,, \\
\hat{s} &= (0, \sin(\theta_c + \gamma), \cos(\theta_c + \gamma))\,, \\
\hat{i} &= (0, -\sin(\theta_c - \gamma), \cos(\theta_c - \gamma))\,, \\
\hat{o_1} &= (\cos\alpha_{P.M.} \cdot \cos(-45^\circ + \theta), \cos\alpha_{P.M.} \cdot \sin(-45^\circ + \theta), \sin\alpha_{P.M.})\,, \\
\hat{o_2} &= (\cos\alpha_{P.M.} \cdot \cos(45^\circ + \theta), \cos\alpha_{P.M.} \cdot \sin(45^\circ + \theta), \sin\alpha_{P.M.})\,,
\end{aligned}
$$

then we have that $\alpha_p^1(\theta)$, $\alpha_p^2(\theta)$, $\alpha_s(\theta)$ and $\alpha_i(\theta)$ are:

$$
\begin{aligned}
&\cos\left(\alpha_p^1(\theta)\right) = \hat{p} \cdot \hat{o_1} \longrightarrow \alpha_p^1(\theta) = \arccos(\cos(\gamma) \cdot \sin\alpha_{P.M.} + \sin(\gamma) \cdot \cos\alpha_{P.M.} \cdot \sin(-45^\circ + \theta)), \\
&\cos\left(\alpha_p^2(\theta)\right) = \hat{p} \cdot \hat{o_2} \longrightarrow \alpha_p^2(\theta) = \arccos(\cos(\gamma) \cdot \sin\alpha_{P.M.} + \sin(\gamma) \cdot \cos\alpha_{P.M.} \cdot \sin(45^\circ + \theta)), \\
&\cos(\alpha_s(\theta)) = \hat{s} \cdot \hat{o_2} \longrightarrow \alpha_s(\theta) = \arccos(\cos(\theta_c + \gamma) \cdot \sin\alpha_{P.M.} + \sin(\theta_c + \gamma) \cdot \cos\alpha_{P.M.} \cdot \sin(45^\circ + \theta)), \\
&\cos(\alpha_i(\theta)) = \hat{i} \cdot \hat{o_2} \longrightarrow \alpha_i(\theta) = \arccos(\cos(\theta_c - \gamma) \cdot \sin\alpha_{P.M.} - \sin(\theta_c - \gamma) \cdot \cos\alpha_{P.M.} \cdot \sin(45^\circ + \theta)).
\end{aligned}
$$

Now, we can compute the relative phase introduced in the wave function:

$$
\begin{aligned}
\phi =& \phi_1 + \phi_2 + \phi_3 + \phi_4 = \\
=& 2\pi \frac{d}{4} \left[\frac{1}{\lambda \cdot \cos\gamma} \left(n^{\text{eff}}(\alpha_p^1(\theta)) - n_o \right) + \left(\frac{1}{\lambda' \cdot \cos(\theta_c + \gamma)} + \frac{1}{\lambda' \cdot \cos(\theta_c - \gamma)} - \frac{1}{\lambda \cdot \cos\gamma} \right) \cdot n_o + \right. \\
&+ \left(\frac{1}{\lambda'} \cdot \left(\frac{n^{\text{eff}}(\alpha_s(\theta))}{\cos(\theta_c + \gamma)} + \frac{n^{\text{eff}}(\alpha_i(\theta))}{\cos(\theta_c - \gamma)} \right) - \frac{1}{\lambda \cdot \cos\gamma} \cdot n^{\text{eff}}(\alpha_p^2(\theta)) \right) \\
&\left. + \left(\frac{1}{\lambda'} \cdot \left(\frac{n^{\text{eff}}(\alpha_s(\theta))}{\cos(\theta_c + \gamma)} + \frac{n^{\text{eff}}(\alpha_i(\theta))}{\cos(\theta_c - \gamma)} \right) - \left(\frac{1}{\lambda' \cdot \cos(\theta_c + \gamma)} + \frac{1}{\lambda' \cdot \cos(\theta_c - \gamma)} \right) \cdot n_o \right) \right] = \\
=& 2\pi \frac{d}{4} \left[\frac{1}{\lambda \cdot \cos\gamma} \cdot \left(n^{\text{eff}}(\alpha_p^1(\theta)) - n^{\text{eff}}(\alpha_p^2(\theta)) - 2 \cdot n_o \right) + \frac{2}{\lambda'} \cdot \left(\frac{n^{\text{eff}}(\alpha_s(\theta))}{\cos(\theta_c + \gamma)} + \frac{n^{\text{eff}}(\alpha_i(\theta))}{\cos(\theta_c - \gamma)} \right) \right].
\end{aligned}
$$

Where $\alpha_e^1(\theta)$ ($\alpha_e^2(\theta)$) is the angle formed between the propagation direction of the extraordinarily polarized pump photons and the optical axis in the first (second) BBO crystal. So:

$$
\boxed{
\begin{aligned}
\phi(\theta) = 2\pi \frac{d}{4} \left[\frac{1}{\lambda \cdot \cos\gamma} \cdot \left(n^{\text{eff}}(\alpha_p^1(\theta)) - n^{\text{eff}}(\alpha_p^2(\theta)) - 2 \cdot n_o \right) + \right. \\
\left. + \frac{2}{\lambda'} \cdot \left(\frac{n^{\text{eff}}(\alpha_s(\theta))}{\cos(\theta_c + \gamma)} + \frac{n^{\text{eff}}(\alpha_i(\theta))}{\cos(\theta_c - \gamma)} \right) \right].
\end{aligned}
} \tag{25}
$$

Assuming the angle γ takes a value of $\gamma = -0.7°$, we can plot the dependence of the angles $\alpha_p^1(\theta)$, $\alpha_p^2(\theta)$, $\alpha_s(\theta)$ and $\alpha_i(\theta)$ as a function of θ, see Fig. 28, as well as the effective refractive index that the photons would experience, i.e., $n^{\text{eff}}(\alpha_p^1(\theta))$, $n^{\text{eff}}(\alpha_p^2(\theta))$, $n^{\text{eff}}(\alpha_s(\theta))$ and $n^{\text{eff}}(\alpha_i(\theta))$, see Fig. 29.

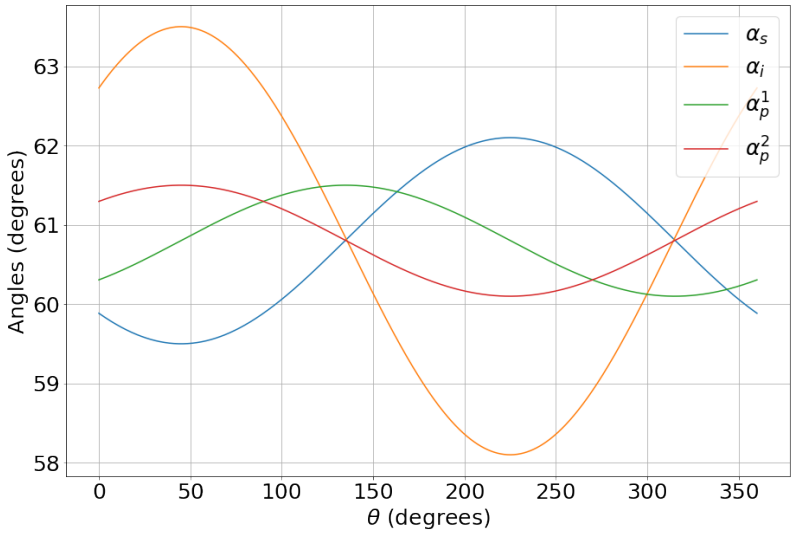

Figure 28: Angle formed by the propagation direction of the pump beam with the optical axis of the first crystal ($\alpha_p^1(\theta)$) and the propagation directions of the pump, signal and idler photons generated in the first crystal with the optical axis of the second crystal ($\alpha_p^2(\theta)$, $\alpha_s(\theta)$ and $\alpha_i(\theta)$) as a function of the rotation angle of the BBO crystals.

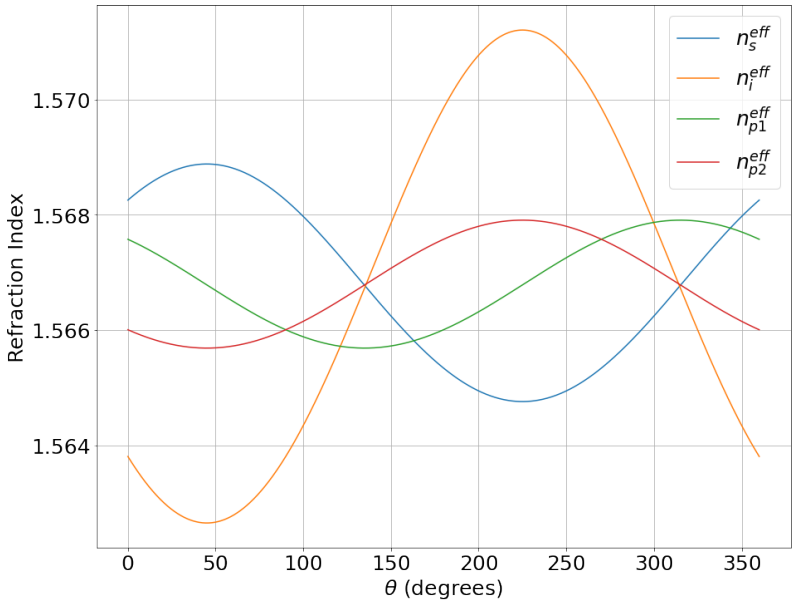

Figure 29: Effective refractive index of the pump photons extraordinary-polarized in the first crystal ($n^{\text{eff}}(\alpha_p^1(\theta))$) and the pump, signal and idler photons extraordinary-polarized in the second crystal ($n^{\text{eff}}(\alpha_p^2(\theta))$, $n^{\text{eff}}(\alpha_s(\theta))$, $n^{\text{eff}}(\alpha_i(\theta))$) as a function of the rotation angle of the BBO crystals.

The relative phase introduced as a function of the crystal angle is shown in Fig. 30.

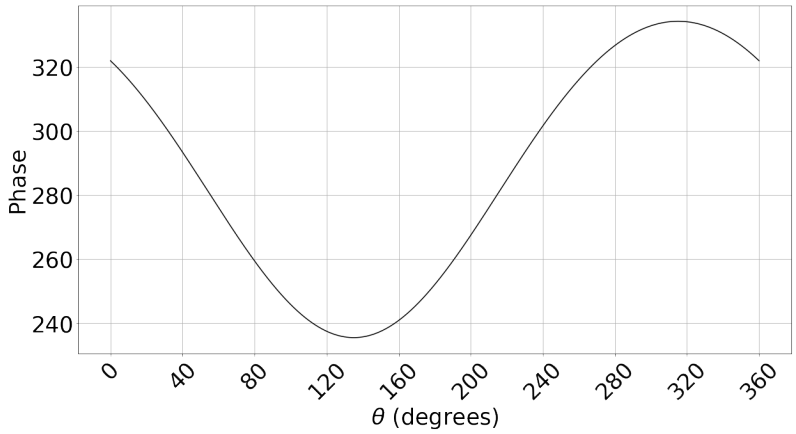

Figure 30: Relative phase between components as a function of the rotation angle of the BBO crystals.

This relative phase does not perfectly fit the data from Fig. 10, possibly because either the refractive index data, crystal thickness, or the value of the angle γ (which we randomly chose to be $-0.7°$) are not exactly correct, or because we are not taking into account some other phenomena or imperfections that contribute to this relative phase.

To consult the Python code that has been used for the calculation of all these graphs, please open the file "RelativePhaseGraphs.ipynb" in the following GitHub repository:

https://github.com/RaulLahoz/RelativePhase

This code also provides us with a plot of the theoretical probabilities for obtaining the photon pairs described by Eq. (8) (where the value of the relative phase is given by Eq. (25)) in the states VV, HH, VH, or HV as a function of the angle θ at which the BBO crystals are located. In this code, we can also vary any of the parameters and see how it affects our relative phase and therefore our probabilities as a function of θ.